NASA CONTRACTOR REPORT NASA CR – 112180

CALCULATION OF HEAT TRANSFER ON SHUTTLE-TYPE CONFIGURATIONS INCLUDING THE EFFECTS OF VARIABLE ENTROPY AT BOUNDARY LAYER EDGE

by Fred R. DeJarnette

Prepared by

MECHANICAL AND AEROSPACE ENGINEERING DEPARTMENT
NORTH CAROLINA STATE UNIVERSITY
RALEIGH, NORTH CAROLINA 27607

for

LANGLEY RESEARCH CENTER
NATIONAL AERONAUTICS AND SPACE ADMINISTRATION
HAMPTON, VIRGINIA 23365

OCTOBER 1972

NASA CR-112180

CALCULATION OF HEAT TRANSFER ON SHUTTLE TYPE CONFIGURATIONS INCLUDING THE EFFECTS OF VARIABLE ENTROPY AT BOUNDARY LAYER EDGE

by Fred R. DeJarnette

Prepared under Contract No. NAS1-10277 by
Mechanical and Aerospace Engineering Dept.
NORTH CAROLINA STATE UNIVERSITY
Raleigh, North Carolina

for Langley Research Center

NATIONAL AERONAUTICS AND SPACE ADMINISTRATION

For sale by the Clearinghouse for Federal Scientific and Technical Information, Springfield, Virginia 22151 - CFSTI price $3.00

Page Intentionally Left Blank

FOREWORD

This research was supported under contract NAS1-10277 with the National Aeronautics and Space Administration's Langley Research Center. The technical monitor on the contract was H. Harris Hamilton. Previous results, without the effect of variable entropy at boundary layer edge, were published in NASA CR 111921 and NASA CR 111922 in August, 1971. This report gives a description of the theoretical approach and changes for the computer program to include the effects of variable entropy at boundary layer edge.

ACKNOWLEDGMENTS

The author would like to express his appreciation to Mr. H. Harris Hamilton, II of the Langley Research Center, NASA for his review of the manuscript and valuable assistance during all phases of this work. In addition, the helpful discussions of Mr. James C. Dunavant of the Langley Research Center, NASA are gratefully acknowledged.

The author would also like to thank the following people at the North Carolina State University:

1. Mr. Michael H. Jones for his assistance in the preparation of this report.
2. Mrs. Joyce Sorensen for typing the manuscript and assisting with the printing.
3. Miss Eleanor Bridgers for her assistance in the printing and assembling of this report.

CONTENTS

CALCULATION OF HEAT TRANSFER ON SHUTTLE TYPE CONFIGURATIONS INCLUDING THE EFFECTS OF VARIABLE ENTROPY AT BOUNDARY LAYER EDGE

by Fred R. DeJarnette
North Carolina State University

October, 1972

SUMMARY

A relatively simple method is presented for including the effect of variable entropy at the boundary-layer edge in a heat transfer method developed previously. For each inviscid surface streamline an approximate shock-wave shape is calculated using a modified form of Maslen's method for inviscid axisymmetric flows. The entropy for the streamline at the edge of the boundary layer is determined by equating the mass flux through the shock wave to that inside the boundary layer. Approximations used in this technique allow the heating rates along each inviscid surface streamline to be calculated independent of the other streamlines.

The shock standoff distances computed by the present method are found to compare well with those computed by Maslen's asymmetric method. Heating rates are presented for blunted circular and elliptical cones and a typical space shuttle orbiter at angles of attack. Variable entropy effects are found to increase heating rates downstream of the nose significantly higher than those computed using normal-shock entropy, and turbulent heating rates increased more than laminar rates. Effects of Reynolds number and angles of attack are also shown.

INTRODUCTION

A relatively simple method was developed in Reference 1 to calculate laminar, transitional and turbulent heating rates on arbitrary blunt-nosed three-dimensional bodies at angle of attack in hypersonic flow. Inviscid surface streamlines were calculated from Euler's equation using a prescribed pressure distribution. Heating rates were determined along a streamline by applying the axisymmetric analog (small cross-flow approximation) for three-dimensional boundary layers to solutions of the axisymmetric boundary-layer equations. In this approximation the distance along a streamline is interpreted as the distance along an equivalent axisymmetric body, and the scale factor (or metric coefficient) for the surface coordinate normal to the streamline (which is a measure of the streamline divergence) is interpreted as the radius of the equivalent axisymmetric body. Thus, each inviscid surface streamline corresponds to a different equivalent body of revolution at zero incidence. In Reference 2 this method was shown to yield accurate laminar heating rates on blunted circular and elliptical cones, and a typical delta-wing space shuttle orbiter at angle of attack.

In the method discussed above the properties at the edge of the boundary layer were determined from the surface pressure and the entropy aft of a normal shock wave (typical blunt body assumption) for an ideal gas or equilibrium air. While this assumption is valid in the nose region of a very blunt bodies, its accuracy decreases as the ratio of distance from the stagnation point to nose radius increases. As the boundary layer along the surface grows, more and more mass is entrained into the boundary layer and it is therefore possible for the boundary layer to swallow the entropy layer.

This means that the streamlines which passed through the nearly normal portion of the bow shock wave are now inside the boundary layer. Although the pressure at the edge of the boundary layer is still nearly the same as that on the surface, the entropy of the streamline at the edge of the boundary layer can be quite different from the normal-shock entropy. As a result, the corresponding heating rate is generally higher than that calculated using the normal-shock entropy.

This report develops an approximate method to include variable entropy at the edge of the boundary layer in the method of References 1 and 2 for calculating heating rates. Modifications needed to combine this addition with the computer program given in Reference 3 are also described. Results are presented for hypersonic flow over blunted circular and elliptical cones and a typical space-shuttle orbiter at angle of attack.

SYMBOLS

a_o, a_1, a_2, a_3	coefficients for geometry of space shuttle orbiter, see eq. (76)
B	ratio of body principal radii of curvature, $R_{T,b}/R_{11,b}$
$\bar{B}$	ratio of shock principal radii of curvature, $\bar{R}_T/\bar{R}_{11}$
$\bar{C}$	parameter used in eq. (18)
$\bar{C}'$	$d\bar{C}/d\bar{\beta}$
D	constant defined by eq. (59)
$\hat{e}_s, \hat{e}_\beta, \hat{e}_n$	unit vectors in shock-oriented coordinate system, eqs. (2), (10), and (11)

$\hat{e}_x, \hat{e}_y, \hat{e}_z$	unit vectors in wind-oriented Cartesian coordinate system
E	constant defined by eq. (60)
f	body radius, ft.
G^2	$1 - \sin^2 \bar{\Gamma}$
h	scale factor in β-direction on body, ft.
$\bar{h}$	scale factor in $\bar{\beta}$-direction on shock, ft.
$\bar{h}_s$	scale factor in $\bar{\xi}$ direction on shock, $d\bar{S} = \bar{h}_s \, d\bar{\xi}$, ft.
h_c	heat transfer coefficient, Btu/ft^2-sec-°R
h_E	reference enthalpy, 2.119×10^8 ft^2/sec^2
h_w	wall enthalpy, ft^2/sec^2
h_2	enthalpy aft of normal shock, ft^2/sec^2
Δh	enthalpy parameter defined by eq. (46), ft^2/sec^2
H	form factor δ^*/θ_m
H_s	stagnation enthalpy, ft^2/sec^2
L	body length, ft.
M	Mach number
n	distance normal to a streamline, ft.
$\bar{n}$	straight line coordinate normal to shock wave and toward body, ft.
p	pressure, lb/ft^2
Δp	pressure parameter defined by eq. (45), lb/ft^2
q_w	heat-transfer rate at wall, Btu/ft^2-sec.
$\bar{q}$	distance normal to $\bar{\beta}$ = constant lines on shock, $d\bar{q} = \bar{h} \, d\bar{\beta}$, ft.
r	radius, ft.
Re/ft	freestream Reynolds number per foot

$Re_{\infty,N}$	freestream Reynolds number based on nose radius
R_N	nose radius, ft.
$R_{T,b}, R_{11,b}$	body principal radii of curvature at stagnation point, ft.
$\vec{R}$	position vector, ft.
$\bar{R}$	shock radius of curvature along $\bar{\beta}$ = constant line, see eq. (43), ft.
$\bar{R}_T, \bar{R}_{11}$	shock principal radii of curvature at stagnation line, ft.
S	distance along inviscid surface streamline, ft.
$\bar{S}$	distance along $\bar{\beta}$ = constant line on shock, ft.
T	temperature, °R
$\bar{u},\bar{v},\bar{w}$	velocity components in $\bar{\xi}$, $\bar{n}$, and $\bar{\beta}$ directions, respectively, ft/sec
V	velocity magnitude, ft/sec
$\vec{V}$	velocity vector, ft/sec
w_f	weighting function
x,y,z	body-oriented coordinate system, see Fig. 14
$\bar{x},\bar{y},\bar{z}$	Cartesian coordinates in wind-oriented coordinate system with origin at the stagnation line of shock wave (see Fig. 1)
x^*	distance defined by eq. (77), ft.
x_1	distance from nose to beginning of body segment, ft.
β	body coordinate normal to inviscid surface streamline
$\bar{\beta}$	shock coordinate normal to $\bar{\xi}$ lines
γ	ratio of specific heats
$\bar{\Gamma}$	shock-wave angle, see eq. (3)

$\bar{\Gamma}_b$	body angle relative to $\vec{V}_\infty$, see eq. (B13)
δ	boundary-layer thickness, ft.
δ^*	boundary-layer displacement thickness, ft.
δ^*_{tr}	transformed displacement thickness, ft.
Δ	shock standoff distance at stagnation line, ft.
$\bar{\epsilon}$	parameter defined by eq. (25), ft.
θ_m	momentum thickness, ft.
θ^*_{tr}	transformed momentum thickness, ft.
ζ_w	wall enthalpy ratio, h_w/H_s
η	$= \Psi/\Psi_{sh}$
Λ	exponent defined by eq. (54)
$\bar{\xi}$	coordinate along shock surface
ρ	mass density, slug/ft^3
$\bar{\sigma}$	angle measured on shock wave, see eq. (4) and Fig. 2
ϕ	body circumferential angle with $\phi = 0$ in windward plane of symmetry
$\bar{\phi}$	shock circumferential angle, $\bar{\phi} = \tan^{-1}(\bar{z}/\bar{y})$
Φ	second stream function, see eq. (7)
Ψ	first stream function, see eq. (7), slugs/sec

Subscripts:

b	body
B.L.	boundary layer
e	edge of boundary layer
lam	laminar

s	stagnation point
sh	at shock wave
turb	turbulent
w	wall
$\bar{\varepsilon}$	evaluated at $\bar{x}_{\bar{\varepsilon}} = \bar{\varepsilon}^2/(2\bar{R}_T)$
2	aft of normal shock
∞	freestream conditions

ANALYSIS

Any highly accurate method which accounts for variable entropy at the edge of the boundary layer would require a complete solution to the three-dimensional inviscid flow field. Such a technique, however, would destroy the simplicity and short computational time that are characteristics of the computer program of Reference 3. Therefore, an approximate, but reasonably accurate, variable entropy method is developed here which is consistent with the other approximations involved in Reference 2.

In order to determine the entropy at the edge of the boundary layer, the position where the edge streamline passed through the shock wave must be determined. Then the slope of the shock wave at this position is all that is needed to calculate the entropy of that streamline. Therefore, a complete knowledge of the inviscid flow field is not needed.

For axisymmetric inviscid flows, Maslen (Ref. 4) developed a simple inverse method based on a von Mises transformation coupled with a simple approximate integral of the lateral momentum equation. Results for several examples were found to compare favorably with those of more exact methods. In particular, the shape of the shock wave and surface pressure distribution (except near the stagnation point) were shown to be very accurate. This method was extended to asymmetric flows in Reference 5; however, only results for the stagnation region of blunt bodies and conical flows were presented in that report. The technique discussed therein for solving the general three-dimensional inviscid flow field is much more complicated than the method developed for axisymmetric flows (Ref. 4). The method described below represents an extension of the axisymmetric Maslen method to general

three-dimensional flows; however, it is much simplier than Maslen's asymmetric method (Ref. 5). The stagnation region will be considered first, since the results can be compared with Maslen's numerical results.

Stagnation Region

As noted by Maslen (Ref. 4), the approximations employed in his method are not strictly valid in the stagnation region; however, for axisymmetric flows it was found to give a reasonably accurate value for the shock standoff distance. For asymmetric flows the requirement is more severe because in addition to a reasonable standoff distance, results should be independent of the direction from which the stagnation line is approached. Maslen's asymmetric solution (Ref. 5) yielded different standoff distances for different directions of approaching the stagnation line. The solution obtained below yields a unique value for the shock standoff distance.

For the stagnation region, it is convenient to use wind-oriented Cartesian coordinates $\bar{x}$, $\bar{y}$, $\bar{z}$ whose origin is located at the normal position on the shock wave with $\bar{x}$ in the direction of $\vec{V}_\infty$ (see Fig. 1). Following Maslen, the shape of the shock wave near the stagnation line is represented by an elliptic paraboloid

$$\bar{x} = \frac{\bar{y}^2}{2\bar{R}_{11}} + \frac{\bar{z}^2}{2\bar{R}_T} \tag{1}$$

where the $\bar{x}$, $\bar{y}$ plane is a plane of symmetry. This equation represents the shock wave by a portion of an ellipsoid for $\bar{x}$ small since the equation is an ellipse in $\bar{y}$ and $\bar{z}$ for $\bar{x}$ = constant. At the origin, the shock radius of curvature is $\bar{R}_{11}$ in the $\bar{x}$, $\bar{y}$ plane and $\bar{R}_T$ in the $\bar{x}$, $\bar{z}$ plane.

The unit (outer) normal to the shock surface is illustrated in Fig. 2 and is given by the relation

$$\hat{e}_{\bar{n}} = \frac{-\hat{e}_{\bar{x}} + \frac{\bar{y}}{\bar{R}_{11}}\hat{e}_{\bar{y}} + \frac{\bar{z}}{\bar{R}_T}\hat{e}_{\bar{z}}}{\left[1 + \left(\frac{\bar{y}}{\bar{R}_{11}}\right)^2 + \left(\frac{\bar{z}}{\bar{R}_T}\right)^2\right]^{1/2}} \tag{2}$$

The slope of the shock wave with respect to the free-stream velocity (shock-wave angle) is $\bar{\Gamma}$, and it is determined from the relation

$$\sin\bar{\Gamma} = -\hat{e}_{\bar{x}} \cdot \hat{e}_{\bar{n}} = \left[1 + \left(\frac{\bar{y}}{\bar{R}_{11}}\right)^2 + \left(\frac{\bar{z}}{\bar{R}_T}\right)^2\right]^{-1/2} \tag{3}$$

In an $\bar{x}$ = constant plane, the angle $\bar{\sigma}$ is defined by

$$\tan\bar{\sigma} = \frac{1}{\bar{B}}\frac{\bar{z}}{\bar{y}} \tag{4}$$

where

$$\bar{B} = \frac{\bar{R}_T}{\bar{R}_{11}} \tag{5}$$

is the ratio of the shock principal radii of curvature at the stagnation line. Using eqs. (3) and (4), eq. (2) can also be written as

$$\hat{e}_{\bar{n}} = -\sin\bar{\Gamma}\,\hat{e}_{\bar{x}} + \cos\bar{\Gamma}\,(\cos\bar{\sigma}\,\hat{e}_{\bar{y}} + \sin\bar{\sigma}\,\hat{e}_{\bar{z}}) \tag{6}$$

The angles $\bar{\Gamma}$ and $\bar{\sigma}$ are illustrated in Fig. 2.

The continuity equation for general three-dimensional flows is automatically satisfied by introducing a pair of stream functions Ψ and Φ such that

$$-\rho V = \nabla\Psi \times \nabla\Phi \tag{7}$$

For the special case of axisymmetric flow the second stream function Φ is identically the circumferential angle $\bar{\phi}$ (where $\tan \bar{\phi} = \bar{z}/\bar{y}$), and hence $\Phi =$ constant planes are $\bar{\phi} =$ constant planes. Streamlines are formed by the intersection of $\Psi =$ constant with $\Phi =$ constant surfaces.

For general three-dimensional flows it is assumed here that inside the shock layer the surface $\Phi =$ constant contains generators which are straight lines normal to the shock wave, and at the shock wave the velocity vector given by the shock relations lies in the $\Phi =$ constant surface. Thus the $\Phi =$ constant surface has the correct shape and slope at the shock wave, but it is not constrained to satisfy all the flow field equations inside the shock layer. For conical flows, this was shown in Reference 5 to be a good approximation except near the body surface. It is believed that this inaccuracy near the body surface has only a small effect on the shape of the shock wave itself. It should be noted that for the applications herein it is the shape of the shock wave that must be reasonably accurate, not the flow field properties inside the shock layer.

Define a three-dimensional shock-oriented coordinate system $\bar{\xi}$, $\bar{\beta}$, $\bar{n}$ where $\bar{\xi}$ and $\bar{\beta}$ are coordinates along the shock surface with $\bar{\beta} \equiv \Phi_{sh}$, and $\bar{n}$ is the straight line normal distance inward from the shock wave. With $\hat{e}_{\bar{s}}$ and $\hat{e}_{\bar{\beta}}$ unit vectors in the directions of $\bar{\xi}$ and $\bar{\beta}$, respectively, the velocity vector becomes

$$\vec{V} = \bar{u}\ \hat{e}_{\bar{s}} + \bar{v}\ \hat{e}_{\bar{n}} + \bar{w}\ \hat{e}_{\bar{\beta}} \tag{8}$$

Since the velocity vector lies in the $\Phi =$ constant surface and $\bar{\beta} \equiv \Phi$, then $\bar{w} \equiv 0$ and

$$\vec{V} = \bar{u}\,\hat{e}_{\bar{s}} + \bar{v}\,\hat{e}_{\bar{n}} \tag{9}$$

At the shock wave, $\hat{e}_{\bar{s}}$, $\hat{e}_{\bar{n}}$, and $\hat{e}_{\bar{\beta}}$ are mutually perpendicular; hence, the direction of $\hat{e}_s$ which makes $\bar{w} = 0$ at the shock is obtained from the shock relations as

$$\hat{e}_{\bar{s}} = \cos\bar{\Gamma}\,\hat{e}_{\bar{x}} + \sin\bar{\Gamma}\,(\cos\bar{\sigma}\,\hat{e}_{\bar{y}} + \sin\bar{\sigma}\,\hat{e}_{\bar{z}}) \tag{10}$$

and thus

$$\hat{e}_{\bar{\beta}} = \hat{e}_{\bar{s}} \times \hat{e}_{\bar{n}} = -\sin\bar{\sigma}\,\hat{e}_{\bar{y}} + \cos\bar{\sigma}\,\hat{e}_{\bar{z}} \tag{11}$$

These results may also be obtained from eqs. (37) and (38) in Reference 1 by setting $\theta = 0$ in those equations. The curve $\bar{n} = 0$, $\bar{\beta}$ = constant on the shock wave represents the locus of points whose tangent is the velocity component parallel to the shock wave. These curves on the shock surface are the same as the simplified streamlines discussed in References 1 and 2, except there the lines were on the body surface instead of the shock wave.

From eqs. (7) and (10) it follows that

$$\rho\bar{u} = -\frac{1}{\bar{h}}\frac{\partial\Psi}{\partial\bar{n}} \tag{12}$$

and

$$\rho\bar{v} = \frac{1}{\bar{h}\,\bar{h}_s}\frac{\partial\Psi}{\partial\bar{\xi}} \tag{13}$$

where $d\bar{S} = \bar{h}_s\,d\bar{\xi}$ is the differential arc length along the $\bar{\xi}$ coordinate, $d\bar{q} = \bar{h}\,d\bar{\beta}$ is the differential arc length along the $\bar{\beta}$ coordinate, and $\bar{h}_s$ and $\bar{h}$ are the scale factors or metric coefficients corresponding to the $\bar{\xi}$ and $\bar{\beta}$ coordinates, respectively.

Comparing eqs (12) and (13) with those for axisymmetric flows (Ref. 6), it is observed that the results here are similar if $\bar{h}$ replaces the axisymmetric body radius and $d\bar{S} = \bar{h}_s \, d\bar{\xi}$ is the distance along the axisymmetric body. Thus, the assumptions made here are somewhat like an axisymmetric alanogue for the invisicd flow field.

The value of the first stream function Ψ on the shock wave represents the mass flux (per unit $\bar{\beta}$) entering the shock layer. The mass flux per unit area is $\rho_\infty V_\infty \sin \bar{\Gamma}$ and the differential of surface area on the shock is $\bar{h} d\bar{\beta} \; \bar{h}_s \, d\bar{\xi}$. Hence the mass flux per unit $\bar{\beta}$ is

$$\Psi_{sh} = \int_o \rho_\infty V_\infty \sin \bar{\Gamma} \; \bar{h} \; \bar{h}_s \, d\bar{\xi} \tag{14}$$

For the special case of axisymmetric flow, $\bar{h} = r_{sh}$, $\sin \bar{\Gamma} \; \bar{h}_s \, d\bar{\xi} = dr_{sh}$ and hence the familiar result

$$\Psi_{sh} = \rho_\infty V_\infty \, r_{sh}^2 / 2$$

is obtained. The shock standoff distance can be obtained by integrating Eq. (12). However, before this integration can be performed, a number of subsidiary relations are needed, and these relations are developed below.

Following the technique used in Reference 1 and 2, equations (10) and (11) are used to obtain the transformation operators

$$\frac{1}{\bar{h}_s} \frac{\partial}{\partial \bar{\xi}} = \cos \bar{\Gamma} \frac{\partial}{\partial \bar{x}} + \sin \bar{\Gamma} \left(\cos \bar{\sigma} \frac{\partial}{\partial \bar{y}} + \sin \bar{\sigma} \frac{\partial}{\partial \bar{z}} \right) \tag{15}$$

and

$$\frac{1}{\bar{h}} \frac{\partial}{\partial \bar{\beta}} = - \sin \bar{\sigma} \frac{\partial}{\partial \bar{y}} + \cos \bar{\sigma} \frac{\partial}{\partial \bar{z}} \tag{16}$$

The line $\bar{\beta}$ = constant on the shock wave follows from Eq. (15) as

$$\frac{\left(\frac{\partial \bar{z}}{\partial \bar{\xi}}\right)}{\left(\frac{\partial \bar{y}}{\partial \bar{\xi}}\right)} = \tan \bar{\sigma} = \frac{1}{\bar{B}} \frac{\bar{z}}{\bar{y}} \tag{17}$$

which integrates to

$$\bar{z}^{\bar{B}} = \bar{C}\, \bar{y} \tag{18}$$

Note that the parameter $\bar{C}$ is a function of $\bar{\beta}$ (on the shock wave).

Equation (18) can be differentiated to give

$$\frac{\partial \bar{\beta}}{\partial \bar{y}} = - \frac{\bar{C}}{\bar{C}' \bar{y}} \tag{19}$$

and

$$\frac{\partial \bar{\beta}}{\partial \bar{z}} = \bar{B} \frac{\bar{C}}{\bar{C}' \bar{z}} \tag{20}$$

where $\bar{C}' = \frac{d\bar{C}}{d\bar{\beta}}$

Using equs. (19) and (20) above, substitute $\bar{\beta}$ into the operator of Eq. (16) to obtain

$$\bar{h} = \frac{\bar{C}'}{\bar{C}^2} \frac{\bar{z}^{-\bar{B}+1}}{\left[\bar{z}^{-2} + \bar{B}^2\, \bar{z}^{2\bar{B}}/\bar{C}^2\right]^{1/2}} \tag{21}$$

Now along the shock wave (with $\bar{\beta}$ = constant);

$$d\bar{S} = \bar{h}_s d\bar{\xi} = \left[(d\bar{x})^2 + (d\bar{y})^2 + (d\bar{z})^2\right]_{\bar{\beta}}^{1/2} \tag{22}$$

$$d\bar{S} = (d\bar{z}/\bar{z})[\bar{z}^2 + \bar{B}^2\,\bar{z}^{2\bar{B}}/\bar{C}^2]^{1/2}\,[1 + (\bar{z}/\bar{R}_T)^2 + (\bar{y}/\bar{R}_{11})^2]^{1/2} \tag{23}$$

Finally, substitute eqs. (4), (21), and (23) into (14) to obtain

$$\Psi_{sh} = \frac{\bar{C}}{\bar{C}^2}\,\frac{\bar{z}^{\bar{B}} + 1}{(\bar{B} + 1)}\,\rho_\infty V_\infty \tag{24}$$

In a manner similar to that of References 1 and 2, the parameter $\bar{C}(\bar{\beta})$ is determined by assigning a value of $\bar{\beta}$ to each line on the shock surface at some point hear the stagnation line (see Fig. 3). This is accomplished by setting

$$\bar{\varepsilon}^2 = 2\,\bar{x}_{\bar{\varepsilon}}\,\bar{R}_T \tag{25}$$

and

$$\bar{\phi}_{\bar{\varepsilon}} = \bar{\beta} \tag{26}$$

Thus at $\bar{x} = \bar{x}_{\bar{\varepsilon}}$ eq. (1) gives

$$\bar{z}_{\bar{\varepsilon}}^2 = \frac{\bar{\varepsilon}^2 \sin^2\bar{\beta}}{\sin^2\bar{\beta} + \bar{B}\cos^2\bar{\beta}} \tag{27}$$

and

$$\bar{y}_{\bar{\varepsilon}}^2 = \frac{\bar{\varepsilon}^2 \cos^2\bar{\beta}}{\sin^2\bar{\beta} + \bar{B}\cos^2\bar{\beta}} \tag{28}$$

Then eq. (24) gives the result (for $\bar{\beta}$ = constant)

$$\frac{\Psi_{sh}}{\Psi_{sh,\bar{\varepsilon}}} = \left(\frac{\bar{z}}{\bar{z}_{\bar{\varepsilon}}}\right)^{\bar{B}+1} \tag{29}$$

where

$$\Psi_{sh,\bar{\varepsilon}} = \frac{(\sin^2\bar{\beta} + \bar{B}^2\cos^2\bar{\beta})\bar{\varepsilon}^2}{(\bar{B}+1)(\sin^2\bar{\beta} + \bar{B}\cos^2\bar{\beta})^2}\rho_\infty V_\infty \tag{30}$$

and

$$\bar{C}(\bar{\beta}) = \frac{\sin^{\bar{B}}\bar{\beta}}{\cos\bar{\beta}}\left(\frac{\bar{\varepsilon}^2}{\sin^2\bar{\beta} + \bar{B}\cos^2\bar{\beta}}\right)^{(\bar{B}-1)/2} \tag{31}$$

With eqs. (3), (18), (27), (28) and (31), $\sin\bar{\Gamma}$ near the stagnation line can be written as

$$\sin\bar{\Gamma} = \left\{1 + \frac{\bar{\varepsilon}^2[(\bar{z}/\bar{z}_{\bar{\varepsilon}})^2\sin^2\bar{\beta} + \bar{B}^2\cos^2\bar{\beta}\,(\bar{z}/\bar{z}_{\bar{\varepsilon}})^{2\bar{B}}]}{(\sin^2\bar{\beta} + \bar{B}\cos^2\bar{\beta})\bar{R}_T^2}\right\}^{1/2} \tag{32}$$

and using eq. (29) it can also be described as

$$\sin\bar{\Gamma} = \left\{1 + \frac{\bar{\varepsilon}^2\left[\sin^2\bar{\beta}\,(\Psi_{sh}/\Psi_{sh,\bar{\varepsilon}})^{2/(\bar{B}+1)} + \bar{B}^2\cos^2\bar{\beta}\,(\Psi_{sh}/\Psi_{sh,\bar{\varepsilon}})^{\frac{2\bar{B}}{\bar{B}+1}}\right]}{\bar{R}_T^2\,(\sin^2\bar{\beta} + \bar{B}\cos^2\bar{\beta})}\right\}^{-1/2} \tag{33}$$

The relation for the stagnation line shock standoff distance Δ follows from eq. (12) as

$$\Delta = \frac{1}{\bar{h}}\int_0^{\Psi_{sh}}\frac{d\Psi}{\rho\bar{u}} = \frac{1}{\rho_2}\int_0^1\frac{d(\Psi/\Psi_{sh})}{(\bar{u}\bar{h}/\Psi_{sh})} \tag{34}$$

Along the stagnation lines both Ψ and Ψ_{sh} are zero. However, the ratio Ψ/Ψ_{sh} approaches a value in the range $0 \leq \Psi/\Psi_{sh} \leq 1$ in the limit as the stagnation line is approached ($\Psi/\Psi_{sh} = 1$ on the shock and $\Psi/\Psi_{sh} = 0$ on the body). Also, the ratio $\bar{u}\bar{h}/\Psi_{sh}$ is indeterminate along the stagnation line, and care must be exercised in evaluating this indeterminancy. The velocity component $\bar{u}$ is obtained from the approximate energy equation used

by Maslen (Ref. 4), i.e.

$$\bar{u}^2 = 2(h_2 - h_e) \tag{35}$$

where h_2 is the static enthalpy aft of normal shock wave and h_e is the local static enthalpy. Since h_e is a function of the pressure and entropy, a Taylor series expansion about the position a streamline crosses the shock wave yields

$$h_e(\bar{\xi},\bar{\beta},\Psi) \simeq h_{sh}(\bar{\beta},\Psi) + \left(\frac{\partial h_e}{\partial p}\right)_{sh} [p(\bar{\xi},\bar{\beta},\Psi) - p_{sh}(\bar{\beta},\Psi)] \tag{36}$$

For isentropic flow along a streamline, the Bernoulli and energy equations give

$$\left(\frac{\partial h_e}{\partial p}\right)_{sh} = \frac{1}{\rho_{sh}(\bar{\beta},\psi)} \tag{37}$$

With $\rho = \rho(p,h_e)$ a Taylor series expansion about the normal shock position produces

$$\frac{1}{\rho_{sh}(\bar{\beta},\Psi)} \simeq \frac{1}{\rho_2} + \left[\frac{\partial(1/\rho)}{\partial p}\right]_2 [p_{sh}(\bar{\beta},\Psi) - p_2] + \left[\frac{\partial(1/\rho)}{\partial h_e}\right]_2 [h_{sh}(\bar{\beta},\Psi) - h_e] \tag{38}$$

In order to determine h_e from eq. (36), an expression for the pressure across the shock layers is needed. The momentum equation normal to a streamline is

$$\frac{\partial p}{\partial n} = \frac{\rho V^2}{R} \tag{39}$$

As in Reference 4, the streamlines are assumed to run parallel to the shock wave in a $\bar{\beta}$ = constant plane; therefore

$$V \simeq \bar{u} \qquad \text{and} \qquad R = \bar{R}$$

Then substituting these results and eq. (12) into eq. (39), the following results is obtained

$$\frac{\partial p}{\partial \Psi} = -\frac{\bar{u}}{\bar{h}\bar{R}} \tag{40}$$

Finally assume $\bar{u}/(\bar{h}\bar{R})$ is constant across the shock layer and equal to its value on the shock wave. Then eq. (40) becomes*

$$\frac{\partial p}{\partial \Psi} = -\frac{u_{sh}}{\bar{h}\bar{R}} \tag{41}$$

Equation (41) integrates to

$$p(\bar{\xi},\bar{\beta},\Psi) = p_{sh}(\bar{\xi},\bar{\beta}) + \frac{u_{sh}(\bar{\xi},\bar{\beta})\Psi_{sh}}{\bar{R}\bar{h}}\left(\frac{\Psi}{\Psi_{sh}} - 1\right) \tag{42}$$

where

$$\bar{R} \equiv -\frac{1}{\left(\frac{\partial \Gamma}{\partial \bar{S}}\right)} \tag{43}$$

is the shock radius of curvature in $\bar{\xi}$ direction. The distinction between $p_{sh}(\bar{\beta},\Psi)$ and $p_{sh}(\bar{\xi},\bar{\beta})$ should be noted in the sketch below.

---

* As noted in Ref. 4, the assumptions leading to eq. (41) introduce compensating errors, and the resulting pressure equation is quite accurate except near the stagnation line.

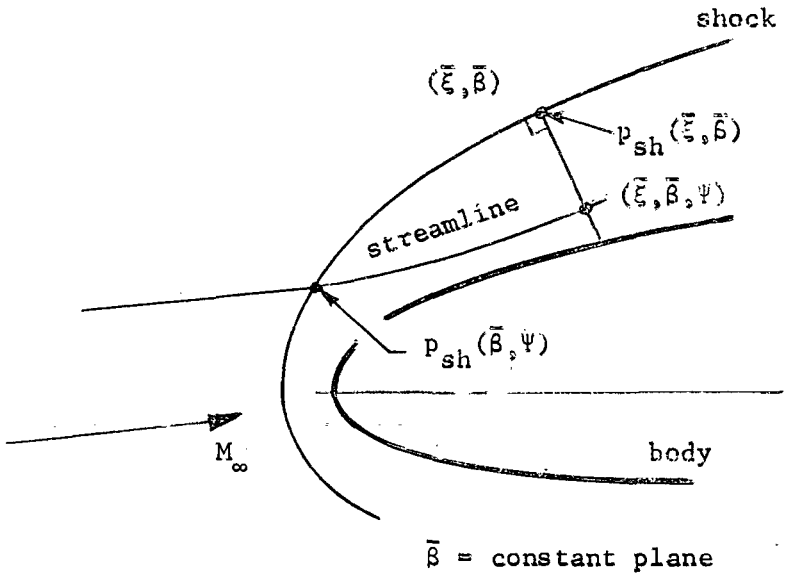

Next, define

$$\sin^2 \bar{\Gamma} \equiv 1 - G^2 \tag{44}$$

$$p_{sh} \equiv p_2 - \Delta p\, G^2 \tag{45}$$

$$h_{sh} \equiv h_2 - \Delta h\, G^2 \tag{46}$$

where near the stagnation line

$$G^2 << 1, \quad \Delta p\, G^2 << p_2, \quad \Delta h\, G^2 << h_2$$

and Δp and Δh depend only on the fluid properties aft of the normal shock wave and are obtained from the shock-wave relations for a perfect gas and equilibrium air in Appendix A. Now, substitute eqs. (36), (37), (38), (42), (45), and (46) into (35), expanding and neglecting the higher order terms;

the following result is obtained

$$u^2(\bar{\xi},\bar{\beta},\Psi) = \frac{2\Delta p}{\rho_2}\left[G^2(\bar{\xi},\bar{\beta}) + \left(\frac{\Delta h \rho_2}{\Delta p} - 1\right) G^2(\bar{\beta},\Psi) + \frac{u_{sh}\,\Psi_{sh}}{\Delta p\,\bar{R}\bar{h}}\left(1 - \frac{\Psi}{\Psi_{sh}}\right)\right] \quad (47)$$

and hence

$$\frac{\bar{h}^2 u^2(\bar{\xi},\bar{\beta},\Psi)}{\Psi_{sh}^2} = \frac{2\Delta p}{\rho_2}\left[\frac{\bar{h}^2 G^2(\bar{\xi},\bar{\beta})}{\Psi_{sh}^2} + \left(\frac{\Delta h \rho_2}{\Delta p} - 1\right)\frac{\bar{h}^2 G^2(\bar{\beta},\bar{\Psi})}{\Psi_{sh}^2} + \frac{u_{sh}\,\bar{h}}{\bar{R}\,\Psi_{sh}}\frac{1}{\Delta p}\left(1 - \frac{\Psi}{\Psi_{sh}}\right)\right] \quad (48)$$

Expanding eq. (32), neglecting the higher order terms, and comparing the result with eq. (44); the following relation is obtained

$$G^2(\bar{\xi},\bar{\beta}) = \frac{\bar{\varepsilon}^2\left[(\bar{z}/\bar{z}_{\bar{\varepsilon}})^2 \sin^2\bar{\beta} + \bar{B}^2\cos^2\bar{\beta}\,(\bar{z}/\bar{z}_{\bar{\varepsilon}})\right]^{2\bar{B}}}{\bar{R}_T^2\,(\sin^2\bar{\beta} + \bar{B}\cos^2\bar{\beta})} \quad (49)$$

In a similar fashion eq. (33) yields

$$G^2(\bar{\beta},\Psi_{sh}) = \frac{\bar{\varepsilon}^2\left[\sin^2\bar{\beta}\,(\Psi_{sh}/\Psi_{sh,\bar{\varepsilon}})^{2/(\bar{B}+1)} + \bar{B}^2\cos^2\bar{\beta}\,(\Psi_{sh}/\Psi_{sh,\bar{\varepsilon}})^{2\bar{B}/(\bar{B}+1)}\right]}{\bar{R}_T^2\,(\sin^2\bar{\beta} + \bar{B}\cos^2\bar{\beta})} \quad (50)$$

This equation is important because it establishes the functional form for $G^2(\bar{\beta},\Psi)$. Replacing Ψ_{sh} with Ψ, it gives

$$G^2(\bar{\beta},\Psi) = \frac{\bar{\varepsilon}^2\left[\sin^2\bar{\beta}\,(\Psi/\Psi_{sh,\bar{\varepsilon}})^{2/(\bar{B}+1)} + \bar{B}^2\cos^2\bar{\beta}\,(\Psi/\Psi_{sh,\bar{\varepsilon}})^{2\bar{B}/(\bar{B}+1)}\right]}{\bar{R}_T^2\,(\sin^2\bar{\beta} + \bar{B}\cos^2\bar{\beta})} \quad (51)$$

Using eqs. (21), (23), (24), (32), (49), and (50) the following results (which are required to integrate eq. (34)) are obtained in the limit as the stagnation line is approched.

$$\lim_{\bar{z}\to 0} \frac{\bar{h}^2 G^2(\bar{\xi},\bar{\beta})}{\Psi_{sh}^2} = \frac{(\bar{B}+1)^2}{\rho_\infty^2 V_\infty^2 \bar{R}_T^2} \tag{52}$$

For every position away from the stagnation line, the ratio Ψ/Ψ_{sh} is unity on the shock wave and zero on the body. Thus, in the limit as the stagnation line is approached ($\bar{z} \to 0$),

$$0 \leq \Psi/\Psi_{sh} \leq 1$$

although both $\Psi \to 0$ and $\Psi_{sh} \to 0$. The remaining terms approach the following limits:

$$\lim_{\bar{z}\to 0} \frac{\bar{h}^2 G^2(\bar{\beta},\Psi)}{\Psi_{sh}^2} = \left[\lim_{\bar{z}\to 0} \frac{\bar{h}^2 G^2(\bar{\xi},\bar{\beta})}{\Psi_{sh}^2}\right]\left[\lim_{\bar{z}\to 0} \frac{G^2(\bar{\beta},\Psi)}{G^2(\bar{\beta},\Psi_{sh})}\right]$$

$$= \frac{(\bar{B}+1)^2}{\rho_\infty^2 V_\infty^2 \bar{R}_T^2} \lim_{\bar{z}\to 0} \frac{\left[\sin^2\bar{\beta}\,(\Psi/\Psi_{sh,\bar{\epsilon}})^{2/(\bar{B}+1)} + \bar{B}^2\cos^2\bar{\beta}\,(\Psi/\Psi_{sh,\bar{\epsilon}})^{2\bar{B}/(B+1)}\right]}{\left[\sin^2\bar{\beta}\,(\Psi_{sh}/\Psi_{sh,\bar{\epsilon}})^{2/(\bar{B}+1)} + \bar{B}^2\cos^2\bar{\beta}\,(\Psi_{sh}/\Psi_{sh,\bar{\epsilon}})^{2\bar{B}/(\bar{B}+1)}\right]}$$

$$= \frac{(\bar{B}+1)^2}{\rho_\infty^2 V_\infty^2 \bar{R}_T^2} (\Psi/\Psi_{sh})^{\Lambda} \tag{53}$$

where

$$\Lambda = \begin{cases} \dfrac{2\bar{B}}{\bar{B}+1} & \text{for} \quad 0 < \bar{B} \leq 1 \\ \dfrac{2}{\bar{B}+1} & \text{for} \quad 1 \leq \bar{B} < \infty \end{cases} \tag{54}$$

Since $\bar{u}_{sh} = V_\infty \cos\bar{\Gamma}$ (from the shock wave relations),

$$\lim_{\bar{z}\to 0} \frac{\bar{u}_{sh}\,\bar{h}}{\bar{R}\,\Psi_{sh}} = -\lim_{\bar{z}\to 0} \frac{\bar{h}\,V_\infty}{\Psi_{sh}} \frac{\partial(\sin\bar{\Gamma})}{\partial\bar{s}} = -\lim_{\bar{z}\to 0} \frac{\bar{h}\,V_\infty}{\Psi_{sh}} \left(\frac{\partial(\sin\bar{\Gamma})}{\partial\bar{z}}\right)_{\bar{\beta}} \frac{\partial\bar{z}}{\partial\bar{s}}$$

$$= +\lim_{\bar{z}\to 0} \frac{(\bar{B}+1)}{\bar{R}_T^2\,\rho_\infty} \frac{\left[\bar{z}^2 + \frac{\bar{B}^3\,\bar{z}^{2\bar{B}}}{\bar{C}^2}\right]}{\left[\bar{z}^2 + \frac{\bar{B}^2\,\bar{z}^{2\bar{B}}}{\bar{C}^2}\right]} \frac{1}{\left[1 + \frac{\bar{z}^2}{\bar{R}_T^2} + \frac{\bar{B}^2\,\bar{z}^{2\bar{B}}}{\bar{C}^2}\right]^2} \tag{55}$$

$$= \begin{cases} \dfrac{(\bar{B}+1)\bar{B}}{\rho_\infty\,\bar{R}_T^2} & \text{for} \quad 0 < \bar{B} \le 1 \\[2ex] \dfrac{(\bar{B}+1)}{\rho_\infty\,\bar{R}_T^2} & \text{for} \quad 1 \le \bar{B} < \infty \end{cases} \tag{56}$$

Finally, substituting eqs. (48) and (51)-(56) into eq. (34) the following equation is obtained for the shock standoff distance

$$\frac{\Delta}{\bar{R}_T} = \left[\left(\frac{\rho_\infty\,V_\infty^2}{2\Delta p}\right)\left(\frac{\rho_\infty}{\rho_2}\right)\right]^{1/2} \frac{1}{(\bar{B}+1)} \int_0^1 \frac{d\eta}{[1 + D(1-\eta) + E\eta^{\Lambda}]^{1/2}} \tag{57}$$

where

$$\eta \equiv \frac{\Psi}{\Psi_{sh}} \tag{58}$$

$$D = \begin{cases} \dfrac{\rho_\infty\,V_\infty^2}{\Delta p} \dfrac{\bar{B}}{\bar{B}+1} & \text{for} \quad 0 < \bar{B} \le 1 \\[2ex] \dfrac{\rho_\infty\,V_\infty^2}{\Delta p} \dfrac{1}{\bar{B}+1} & \text{for} \quad 1 \le \bar{B} < \infty \end{cases} \tag{59}$$

and,

$$E = \frac{\Delta h}{V_\infty^2} \frac{\rho_2}{\rho_\infty} \frac{\rho_\infty\,V_\infty^2}{\Delta p} - 1 \tag{60}$$

Expression for $\frac{\Delta p}{\rho_\infty V_\infty^2}$ and $\frac{\Delta h}{V_\infty^2}$ are given in Appendix A for both an ideal gas and equilibrium air. For an ideal gas the results from Appendix A are

$$\frac{\Delta p}{\rho_\infty V_\infty^2} = \frac{2}{\gamma+1}$$

and

$$E = \frac{(M_\infty^2 - 1)^2}{2M_\infty^2(1 + \frac{\gamma-1}{2} M_\infty^2)}$$

In general, eq. (57) cannot be integrated in closed form. However, for the special case of $\bar{B} = 1$ (spherical shock at stagnation line) it can be integrated to yield the same result given by Maslen in Ref. 4, i.e.

$$\frac{\Delta}{\bar{R}} = \left[\left(\frac{\rho_\infty V_\infty^2}{2\Delta p}\right) \frac{\rho_\infty}{\rho_2}\right]^{1/2} \frac{1}{\left[(1 + E)^{1/2} + \left(1 + \frac{\rho_\infty V_\infty^2}{2 p}\right)^{1/2}\right]} \tag{61}$$

which compares well with more exact numerical results and experimental data.

Shock Shape Downstream of Stagnation Region

In reference 1 a method is developed for calculating the inviscid surface streamlines from a prescribed pressure distribution assuming "normal shock" entropy at the edge of the boundary layer. Before the entropy at the edge of the boundary layer can be calculated, the shock-wave shape associated with each inviscid surface streamline must be determined. Normally, the entire shock shape in the subsonic-transonic region would have to be determined iteratively. However, it is assumed here that for a given surface

pressure distribution the shock shape associated with each inviscid surface streamline can be calculated independently of the others. This procedure highly simplifies the calculations and is consistent with the accuracy of the assumptions used in Reference 1.

For the region downstream of the stagnation line, it is assumed that $\bar{\beta} = \beta$, i.e. a $\bar{\beta}$ = constant plane is assumed to intersect the body surface on a line of β = constant which is an inviscid surface streamline. With this assumption, eq. (42) can be applied to the surface to give

$$p_b(\bar{\xi},\bar{\beta}) \simeq p_{sh}(\bar{\xi},\bar{\beta}) - \frac{\bar{u}_{sh}(\bar{\xi},\bar{\beta})\ \Psi_{sh}}{\bar{R}\ \bar{h}} \tag{63}$$

Then using eq. (43)

$$\frac{\bar{u}_{sh}\ \Psi_{sh}}{\bar{R}\ \bar{h}} = -\frac{V_\infty\ \Psi_{sh}}{\bar{h}}\ \frac{\partial(\sin\bar{\Gamma})}{\partial\bar{S}} - \frac{V_\infty\ \Psi_{sh}}{h}\ \frac{\partial(\sin\bar{\Gamma})}{\partial S} \tag{64}$$

where h is the scale factor for the coordinate β on the body surface and S is distance along an inviscid surface streamline.

Now substitute eq. (64) into (63) to obtain

$$\frac{\partial(\sin\bar{\Gamma})}{\partial S} = (p_b - p_{sh})\ \frac{h}{V_\infty\ \Psi_{sh}} \tag{65}$$

This equation can be integrated numerically along an inviscid surface streamline to determine the value of $\sin\bar{\Gamma}$ (where $\bar{\Gamma}$ is the shock angle) associated with each position. The value of Ψ_{sh} for each position can be calculated numerically from eq. (14) in the following form

$$\Psi_{sh} = \rho_\infty V_\infty \int_0 \sin\bar{\Gamma}\ \bar{h}d\bar{S} \simeq \rho_\infty V_\infty \int_0 \sin\bar{\Gamma}\ h dS \tag{66}$$

Thus for each position along an inviscid surface streamline the corresponding values of $\bar{\Gamma}$ and Ψ_{sh} are known. As will be shown below, the value of $\bar{\Gamma}$ (shock-wave angle) corresponding to a given value of Ψ_{sh} is all that is needed to determine the entropy at the edge of the boundary layer. The surface pressure distribution used in eq. (65) must be modified so that $p_b = p_{sh}$ at the stagnation line instead of the stagnation pressure. For a given surface pressure (p_e) distribution which yields $p_e = p_{stag}$ at the stagnation line, this can be accomplished by simply using

$$p_b = p_\infty + (p_e - p_\infty) \frac{(p_2 - p_\infty)}{(p_s - p_\infty)} \tag{67}$$

where p_b is the pressure to be used in eq. (65) only.

Entropy at the Edge of the Boundary Layer

The mass flux within the boundary layer along an inviscid surface streamline is

$$\rho_e u_e h \, d\beta \, (\delta - \delta^*)$$

where $\rho_e u_e (\delta - \delta^*)$ is the mass flux per unit width and $h d\beta$ is the spacing between inviscid surface streamlines.

Therefore the mass flux per unit β is

$$\Psi_{B.L.} = \rho_e u_e h (\delta - \delta^*) \tag{68}$$

where δ is the boundary layer thickness and δ^* is the displacement thickness. Now the streamline at the edge of the boundary layer passed through the bow shock wave at the position where

$$\Psi_{sh} = \Psi_{B.L.} \tag{69}$$

or, in other words, where the mass flux (per unit β) inside the boundary layer is equal to the mass flux (per unit β) entering the shock wave (see sketch below).

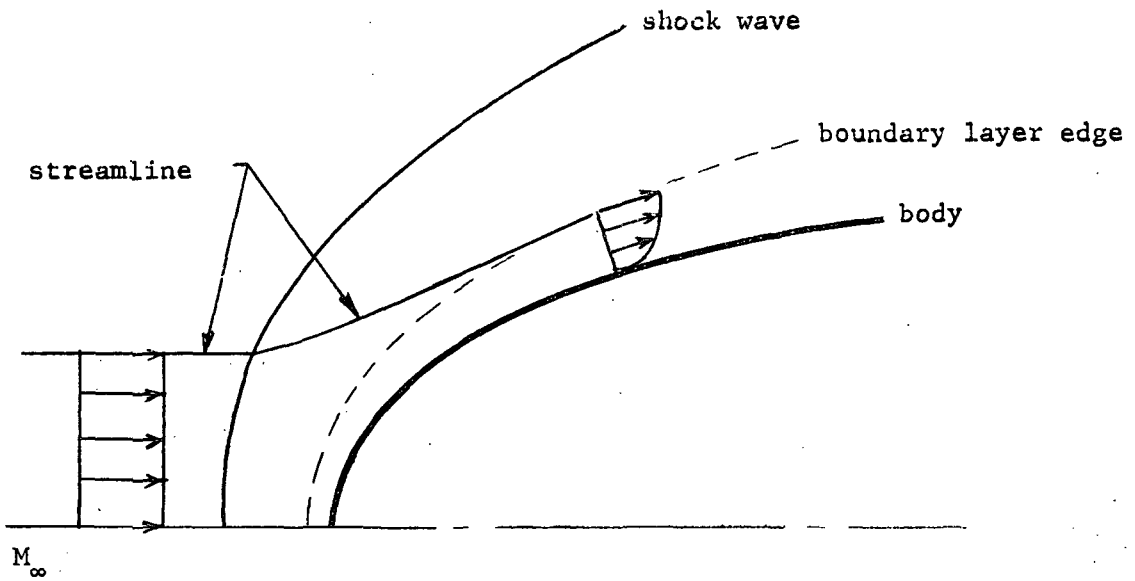

β = constant plane

Then for the value of Ψ_{sh} given by eq. (69), the shock angle $\bar{\Gamma}$ is determined by the method developed in the previous section. After $\bar{\Gamma}$ is

determined, it is a relatively simple matter to calculate the entropy for that streamline from the shock relations.

The procedure described above must generally be performed iteratively because the properties on the right side of eq. (68) require both the pressure and entropy at the edge of the boundary layer. Since the entropy is not known initially, a value of normal shock entropy (or value for last station along that surface streamline) could be used to start the iteration. Convergence is quite fast and generally requires less than four iterations.

Calculation of $\delta - \delta^*$

Laminar Boundary Layer

In reference 1 a method was given for calculating the momentum thickness θ_m based on applying the axisymmetric analogue to Beckwith and Cohen's boundary layer results (ref. 8). Following the technique of reference 8, it follows that

$$\delta - \delta^* = \theta_m\left(\frac{\delta - \delta^*}{\theta_m}\right) = \theta_m\left(\frac{\delta_{tr} - \delta^*_{tr}}{\theta^*_{tr}}\right) \tag{70}$$

and from Table 1 in reference 8

$$\theta^*_{tr} = .4696 \quad \text{and} \quad \delta^*_{tr} = 1.2168$$

In addition, it is assumed that $\delta^*_{tr} = 5.2/\sqrt{2}$, corresponding to the factor 5.2 used to define the edge of the boundary layer in the Blasius solution for a flat plate. Using these results, eq. (70) becomes

$$\delta - \delta^* = 5.27\ \theta_m \tag{71}$$

for the laminar boundary layer.

Turbulent Boundary Layer

In reference 1 the turbulent boundary layer theory of Reshotko and Tucker (ref. 9) was used. Following the method of Ref. 9,

$$\delta - \delta^* = \theta_m\left(\frac{\delta}{\theta_m} - H\right) = \theta_m\left(\frac{\delta_{tr}}{\theta_{tr}} - H\right) \tag{72}$$

Then with a 1/7 power law for the transformed incompressible velocity profile, it follows that

$$\frac{\delta_{tr}}{\theta_{tr}} = \frac{(7+1)(6+2)}{7} = 10.3$$

Using this result in eq. (72) the following relation for $\delta - \delta^*$ is obtained

$$\delta - \delta^* = \theta_m\,(10.3 - H) \tag{73}$$

for the turbulent boundary layer. The form factor $H \equiv \delta^*/\theta_m$ is calculated by the method described in reference 1.

Transition Region

For the transition region, the weighting function w_f used in reference 1 is used to give an average value of $\delta - \delta^*$ as

$$\delta - \delta^* = (1 - w_f)5.27\ \theta_{m,lam} + w_f\ \theta_{m,turb}\ (10.3 - H) \qquad (74)$$

where $w_f = 0$ for laminar and $w_f = 1$ for turbulent flows.

Method for Calculation

The technique described in this report is coupled with that of reference 1 to calculate the heat transfer rate with variable entropy at the edge of the boundary layer. Appendix A describes the method used to determine $\bar{B}$ and $\bar{R}_T$ on the shock wave at the stagnation line which correspond to the body shape (B and R_T for the body differ from the corresponding quantities on the shock wave). The changes needed for the computer program listed in reference 3 to be modified to include variable entropy at the edge of the boundary layer are given in Appendix C.

RESULTS AND DISCUSSION

Table 1 shows a comparison of the stagnation line standoff distances computed by the present method, eq. (57), and Maslen's method (ref. 5). Maslen obtained different results depending on the direction that the stagnation line was approached. Thus the r.m.s. value is given with the r.m.s. deviation from that value. This table shows that the present method compares well with Maslen's for the stagnation standoff distance.

Figure 4 gives the variation of $\Delta/\bar{R}_T$ with $\bar{B}$ for $M_\infty = 2$, 5, and 10. As expected, the differences between the $M_\infty = 5$ and 10 results are small.

Blunted 15° Half-Angle Circular Cone

Laminar heating rates were calculated along the windward plane of symmetry of a spherically blunted ($R_N = 0.375$ in.) 15° half-angle circular cone at $M_\infty = 10.6$, $\alpha = 20°$, and $Re_{\infty,N} = 3.75 \times 10^4$. Since the nose radius is a significant parameter for variable entropy effects, the Reynolds number $Re_{\infty,N}$ is based on the nose radius of the body. In order to compare the numerical results with Cleary's tabulated experimental data (Ref. 10), the free-stream properties corresponding to wind-tunnel stagnation properties of $p_s = 1.728 \times 10^5$ lb/ft^2 and $T_s = 2000°R$ were calculated to be $p_\infty = 2.6614$ lb/ft^2, $T_\infty = 89.971°R$, and $V_\infty = 4928.1$ ft/sec ($M_\infty = 10.6$). Also, it was determined that a value of $\zeta_w \equiv h_w/H_s = 0.251$ corresponds to $T_w/T_s = 0.270$. Gas imperfections in the wind-tunnel stagnation properties were taken into account in determining the free-stream conditions; however, the laminar heating rates were calculated using a perfect gas with $\gamma = 1.4$.

The experimental heating rates in Ref. 10 are ratioed to the calculated value of $q_{w,s}$ = 35.94 Btu/ft^2-sec in this report.

Figures 5 and 6 compare the calculated ratio of local to stagnation-point heat-transfer rate along the windward plane of symmetry with the experimental data. In each figure numerical results are presented for both variable entropy and normal-shock entropy along the edge of the boundary layer. Figure 5 gives the heating-rate ratios using inviscid surface streamlines calculated from modified Newtonian pressures. When the variable entropy effect is included, these streamlines can differ significantly from those calcualted using normal-shock entropy. Thus, there are essentially two factors involved in the variable entropy effects on the heating rate - one is the scale factor associated with the streamlines and the second is the flow-field properties at the edge of the boundary layer. The first factor tends to decrease the heating rate when the scale factor decreases, whereas the second factor tends to increase the heating rate where variable entropy effects are significant. In Figure 5 the heating rates calculated with variable entropy effects are slightly below those calcualted with normal-shock entropy. Upon examining the numerical results it was found that the variable entropy effect reduced the streamline scale factor h along the windward plane of symmetry which, in turn, reduced the heating-rates slightly more than the increase in heating-rates due to the variable entropy effect on the flow-field properties at the edge of the boundary layer.

Figure 6 shows the calculated heating-rate ratios using the simplified streamline patterns discussed in Ref. 1. The simplified streamlines depend

on the body geometry and angle of attack only; hence, variable entropy has no effect on the geometry of the simplified streamlines and their corresponding scale factors. As a result, the variable entropy effect increased the heating-rate ratios in Figure 6 about 15% higher than those calculated using normal-shock entropy. The experimental data fell between the two theoretical solutions.

The heating rates for the cases presented in Figures 5 and 6 were also calculated using tangent wedge and tangent cone pressures along the conical afterbody in lieu of that given by eq. (67). However, no discernible differences could be detected when the results were plotted on Figures 5 and 6, and therefore they are not shown.

Blunted 2:1 Elliptical Cone

Laminar heating rates were also calculated on a blunted 2:1 elliptical cone at $\alpha = 15°$, 30°, and 60°; $M_\infty = 10$; and $Re_{\infty,N} = 2.61 \times 10^4$, 8.39×10^4, and 2.02×10^5. Figure 7 illustrates the geometry of the model used for the experimental heat-transfer data presented in Ref. 11. The pertinent flow-field properties required as input data for each case calculated in this report are presented in Table 2. All lengths and Reynolds numbers ($Re_{\infty,N}$) are referenced to the nose radius in the plane of the major axis ($R_N = 1.0$ in.). As noted in Ref. 2, modified Newtonian pressures are not accurate enough to give the proper spreading of the streamlines (and hence the correct scale factor) for this body shape. Therefore, the simplified streamlines discussed in Ref. 1, which depend on

body geometry and angle of attack only, are used in each case presented herein.

Figure 8 shows the heating-rate ratio along the windward plane of symmetry for $Re_{\infty,N} = 8.39 \times 10^4$ and $\alpha = 15°$, $30°$, and $60°$. Downstream of the nose the variable entropy effect increased the heating rate ratio about 10% for $\alpha = 15°$, 20% for $\alpha = 30°$, and 30% for $\alpha = 60°$ over that calculated using normal-shock entropy. These percentages tended to remain constant in the downstream region. Heating rates calculated with variable entropy agree much better with the experimental data than those calculated with normal-shock entropy. The effects of variable entropy on the heating rates begin closer to the nose for the larger angles of attack cases.

The effect of Reynolds number on the laminar heating-rate ratio with variable entropy is depicted in Figure 9 for the windward plane of symmetry on the blunted 2:1 elliptical cone at $\alpha = 30°$. Since the boundary layer thickness increases as the Reynolds number decreases, the effect of variable entropy on the heating rate begins closer to the nose for the smaller Reynolds numbers. This effect can also be observed in Figure 10 which shows the variation of the shock angle corresponding to the position where the streamline at the edge of the boundary layer crossed the shock wave. This shock angle decreases downstream of the nose with the smallest Reynolds number case decreasing the fastest. For $x/R_N \geq 10$ the shock-wave angle for all three Reynolds number cases approaches the straight portion of the shock wave surrounding the conical afterbody in the windward plane of symmetry.

Figures 11 and 12 show the circumferential variation of the heat transfer coefficient on the blunted 2:1 elliptical cone at $\alpha = 30°$ and 60°, respectively, for the axial positions of $x/R_N = 4.7$ and 9.7. The heat transfer coefficients calculated with variable entropy effects agree much closer with the experimental data than those with normal-shock entropy on the windward surface. However, very little difference was found for the leeward region. Figure 13 shows the circumferential variation in the shock-wave angle corresponding to the streamline at the edge of the boundary layer at axial stations of $x/R_N = 2.2$, 4.7, and 9.7. These results show that the shock angle decreases going away from the windward plane ($\phi=0$), reaches a minimum value near $\phi = 100°$, and then increases as the leeward plane ($\phi=180°$) is approached.

Space Shuttle Orbiter

Figure 14 shows a typical space shuttle orbiter (without a canopy) on which computations have been performed. The analytical description is similar to that given in Ref. 12; it employs elliptical cross-sectional shapes with different ellipticity ratios on windward and leeward sides. Cubic polynominals are used to define the plan and thickness distributions. Based on a length of $L = 1$ ft., the region for $x/L \leq 0.05$ is a spherically blunted 15° cone whose nose radius is $R_N/L = 0.01512$. For $0.05 \leq x/L \leq 1.0$, the body shape is the same as that in Ref. 12 where the body radius $f(x,\phi)$ is given by

$$f(x,\phi) = y[\cos^2 \phi + (y/z)^2 \sin^2 \phi]^{-1/2} \tag{75}$$

where

$$\left.\begin{matrix} y \\ z \end{matrix}\right\} = a_o + a_1 x^* + a_2 x^{*2} + a_3 x^{*3} \tag{76}$$

$$x^* = x - x_1 \tag{77}$$

and the coefficients for the equations above are given in Table 3 for five body segments. This description of the body produces continuous body slopes but discontinuous radii of curvature.

As noted in Ref. 2, since the windward side of this vehicle is nearly flat the modified Newtonian pressure distribution does not give an accurate description of the inviscid surface streamlines. Therefore, the results presented here calculated the streamlines by the simplified method given in Ref. 1, which depends only on the body geometry and angle of attack. The following properties were used for all the calculations: $p_\infty = 2.2766$ lb/ft^2, $T_\infty = 87.31°R$, $V_\infty = 4639.42$ ft/sec, ($M_\infty = 10.13$, $Re_{\infty,N} = 1.5 \times 10^4$), $\zeta_w = 0.2501$, and $\gamma = 1.4$.

Figure 15 shows the laminar heating-rate ratio along the windward plane for $\alpha = 15°$, 30°, and 60°. The trend here is somewhat similar to the blunted 2:1 elliptical cone in that the variable entropy effects increase the heating-rate ratio more at the larger angles of attack. Figures 16, 17, and 18 illustrate the circumferential heating-rate ratio at $x/L = 0.1$, 0.3, and 0.5, respectively. These figures show that the variable entropy effects on the heating are significant on the windward side but insignificant on the leeward side. Figures 17 and 18 also show that

the heating-rate ratio reaches a maximum off the windward plane of symmetry for $x/L = 0.3$ and 0.5.

Heating-rate ratios for laminar, transitional, and turbulent heating along the windward plane of symmetry are presented in Figures 19 (a) & (b) for $\alpha = 15°$ and $30°$, respectively. The transition region was arbitrarily chosen to be $0.55 \leq x/L \leq 0.80$. These figures show that variable entropy effects on the heating are much more pronounced in the turbulent region than the laminar religion. For $\alpha = 30°$, the increase in the calculated heating-rate ratio with variable entropy over that for normal-shock entropy is about 10% for the laminar region whereas it is about 50% in the turbulent region.

CONCLUDING REMARKS

A relatively simple method is presented for modifying the heat transfer method developed in References 1-3 to include the effects of variable entropy at the edge of the boundary layer. An approximate shock-wave shape corresponding to each inviscid surface streamline is calculated using a modified form of Maslen's method for inviscid axisymmetric flows (Ref. 4). The position where the streamline at the edge of the boundary layer crosses the shock wave is determined by equating the mass flux passing through the shock wave to that inside the boundary layer. The slope of the shock wave at that position determines the entropy of that streamline. The approximations used in this technique allow the shock-wave shape

and surface heating rates corresponding to each inviscid surface streamline to be calculated independent of the other streamlines.

The approximate inviscid solution used to generate the shock-wave shape is based on Maslen's observation that most of the mass flow inside the shock layer is concentrated near the shock. Hence, it is assumed that across the shock layer the streamlines are essentially parallel to the shock and have the same direction as the velocity vector just aft of the shock wave. This assumption is somewhat like an axisymmetric analog for the inviscid flow field. Although the approximations involved are inaccurate near the surface, they appear to have little effect on the shape of the shock wave itself. It is the shape of the shock wave that is needed here and not a detailed structure of the flow-field properties across the shock layer.

The shock standoff distances given by the present method compare well with those computed by Maslen's more elaborate asymmetric method (Ref. 5). In order to make the computation of the shock shape downstream of the nose a direct one, an approximate surface pressure distribution (eq. (67)) was used. This distribution was found to yield accurate shock shapes for a sphere, but it has not been checked for other body shapes. If the surface pressure distribution was not specified, the shock shape solution would have to be solved by an iterative scheme.

The calculated laminar heating rates on blunted circular and elliptical cones showed that the effects of variable entropy were significant on the windward side but insignificant on the leeward side. At both $\alpha = 30°$ and $60°$ the calculated heating rates on the blunted 2:1 elliptical

cone were very close to the experimental data with variable entropy, whereas the heating rates with normal-shock entropy were significantly lower than the experimental results on the windward side. It was found that variable entropy effects started nearer the nose for those cases calculated at the lower Reynolds number. The percentage increase in laminar heating rates due to variable entropy effects was also higher at the larger angles of attack.

The calculated heating rates on a typical space shuttle orbiter showed that variable entropy effects were significant over a large portion of windward plane of symmetry. In addition, variable entropy effects increased the calculated turbulent heating rates much more than it did for the laminar heating rates. However, comparisons with experimental turbulent heating rates are needed to assess the accuracy of the present method.

The method presented here requires comparatively small computational time. A typical case requires only a few seconds per streamline on the IBM 370/165 computer.

APPENDIX A

DERIVATION OF Δp AND Δh

The oblique shock-wave relations for an equilibrium or ideal gas are:

$$\rho_\infty V_\infty \sin \bar{\Gamma} = \rho_{sh} V_{sh} \tag{A1}$$

$$p_\infty + \rho_\infty V_\infty^2 \sin^2 \bar{\Gamma} = p_{sh} + \rho_\infty V_\infty \sin \bar{\Gamma} V_{sh} \tag{A2}$$

$$h_\infty + \frac{V_\infty^2 \sin^2 \bar{\Gamma}}{2} = h_{sh} + \frac{V_{sh}^2}{2} \tag{A3}$$

Substitute $\sin^2 \bar{\Gamma} = 1 - G^2$, $p_{sh} = p_2 - \Delta p G^2$, $h_{sh} = h_2 - \Delta h\, G^2$ (where $G^2 << 1$), and eq. (38) into the above equations. Neglecting terms of order higher than G^2, the following results are obtained:

$$\frac{\Delta p}{\rho_\infty V_\infty^2} = \frac{(\rho_\infty/\rho_2 - 1)\left[\frac{\rho_\infty V_\infty^2}{2} \frac{\partial(1/\rho)}{\partial h_e} (1 - \rho_\infty/\rho) - 1\right]_2}{1 + \rho_\infty^2 V_\infty^2 \left[\frac{\partial(1/\rho)}{\partial p} + \frac{1}{\rho} \frac{\partial(1/\rho)}{\partial h_e}\right]_2} \tag{A4}$$

and

$$\frac{\Delta h}{V_\infty^2} = \frac{\left(\frac{\rho_\infty}{\rho_2} - 1\right)\left[\frac{\rho_\infty^3 V_\infty^2}{\rho} \frac{\partial(1/\rho)}{\partial p} - \frac{1}{2}\left(\frac{\rho_\infty}{\rho_2} + 1\right)\left(1 + \rho_\infty^2 V_\infty^2 \frac{\partial(1/\rho)}{\partial p}\right)\right]_2}{1 + \rho_\infty^2 V_\infty^2 \left[\frac{\partial(1/\rho)}{\partial p} + \frac{1}{\rho} \frac{\partial(1/\rho)}{\partial h_e}\right]_2} \tag{A5}$$

For the special case of an ideal gas,

$$\frac{1}{\rho} = \left(\frac{\gamma - 1}{\gamma}\right) \frac{h_e}{p} \tag{A6}$$

$$\frac{\partial(1/\rho)}{\partial p} = -\frac{1}{\rho p} \tag{A7}$$

and

$$\frac{\partial(1/\rho)}{\partial h_e} = \left(\frac{\gamma-1}{\gamma p}\right) \tag{A8}$$

Then using the normal shock relations to obtain expressions for p_2, ρ_2, and h_2 and substituting eqs. (A6)-(A8) into eq. (A4) yields

$$\frac{\Delta p}{\rho_\infty V_\infty^2} = \frac{2}{\gamma+1} \tag{A9}$$

Further, combining eqs. (A5) and (A9) and using eqs. (A6)-(A8) yields the following result for the ideal gas

$$E \equiv \frac{\Delta h}{V_\infty^2} \frac{\rho_2}{\rho_\infty} \frac{\rho_\infty V_\infty^2}{\Delta p} - 1 = \frac{(M_\infty^2 - 1)}{2M_\infty^2 \left(1 + \frac{\gamma-1}{2} M_\infty^2\right)} \tag{A10}$$

For equilibrium air, the correlation formulae of Reference 7 are also used here to be consistent with the approach taken in Ref. 1. The expression for the reciprocal of the density is (Ref. 7)

$$\frac{1}{\rho} = \frac{1 - 1.0477\left[1 - (h_e/h_E)^{.6123}\right]}{7.344 \times 10^5 \left(\frac{p}{2117}\right)^{.965}} \tag{A11}$$

where

$$h_E = 2.119 \times 10^8 \text{ ft}^2/\text{sec}^2 \tag{A12}$$

From the above equation the following expressions are obtained

$$\left[\frac{\partial(1/\rho)}{\partial p}\right]_2 = -\frac{.965}{p_2 \rho_2} \tag{A13}$$

and

$$\left[\frac{\partial(1/\rho)}{\partial h_e}\right]_2 = \frac{(1.0477)(.6123)(h_2/h_E)^{.6123}}{h_2\ 7.344 \times 10^{-5}\ \left(\frac{p_2}{2117}\right)^{.965}} \qquad (14)$$

The normal shock poperties p_2, ρ_2 and h_2 are calculated by the iterative technique described in Reference 1. Note that any other equilibrium gas model could also be used in lieu of the one described above.

APPENDIX B

RELATIONSHIP BETWEEN SHOCK AND BODY RADII OF CURVATURE AT STAGNATION LINE

The expression for $\Delta/\bar{R}_T$ given by eq. (57) requires the shock radii of curvature ($\bar{R}_T$ and either $\bar{B}$ or $\bar{R}_{11}$) to be known at the stagnation line before the standoff distance Δ can be calculated. For blunt-nosed bodies, this would generally require an iterative solution for the entire subsonic-transonic region before $\bar{R}_T$ and $\bar{B}$ could be determined. On the other hand, these quantities can be calculated if a surface pressure distribution, consistent with eq. (42), is known in the vicinity of the stagnation line. For the analysis herein, a surface pressure distribution similar to modified Newtonian pressures is used for calculating the shock wave shape. This pressure distribution is

$$p_b = (p_2 - p_\infty) \sin^2 \bar{\Gamma}_b + p_\infty \tag{B1}$$

where $\bar{\Gamma}_b$ is the inclination of the body surface with respect to the free-stream velocity ($\bar{\Gamma}_b = \pi/2$ at stagnation point). Note that this equation is a modification of modified Newtonian pressures in order to give $p_b = p_2$ at the stagnation point, which is required to be consistent with eq. (42). Equation (42) also gives the surface pressure (by substituting $\Psi = 0$) as

$$p_b = p_{sh}(\bar{\xi},\bar{\beta}) + \frac{\Psi_{sh}\, \bar{u}_{sh}(\bar{\xi},\bar{\beta})}{\bar{R}\, \bar{h}} \tag{B2}$$

Equating the right sides of eqs. (B1) and (B2), there results

$$(p_2 - p_\infty)\ \sin^2 \bar{\Gamma}_b + p_\infty = p_{sh}(\bar{\xi},\bar{\beta}) - \frac{\Psi_{sh}\ \bar{u}_{sh}(\bar{\xi},\bar{\beta})}{\bar{R}\ \bar{h}} \qquad \text{(B3)}$$

Equation (B3) will give the desired relationship between shock and body radii of curvature; however, the body points $(\bar{y}_b, \bar{z}_b)$ corresponding to shock points $(\bar{y}, \bar{z})$ must be established first.

Let $\vec{R}_{sh}$ be the position vector for a shock point and $\vec{R}_b$ the corresponding body point in the wind-oriented coordinate system, as shown in the sketch below.

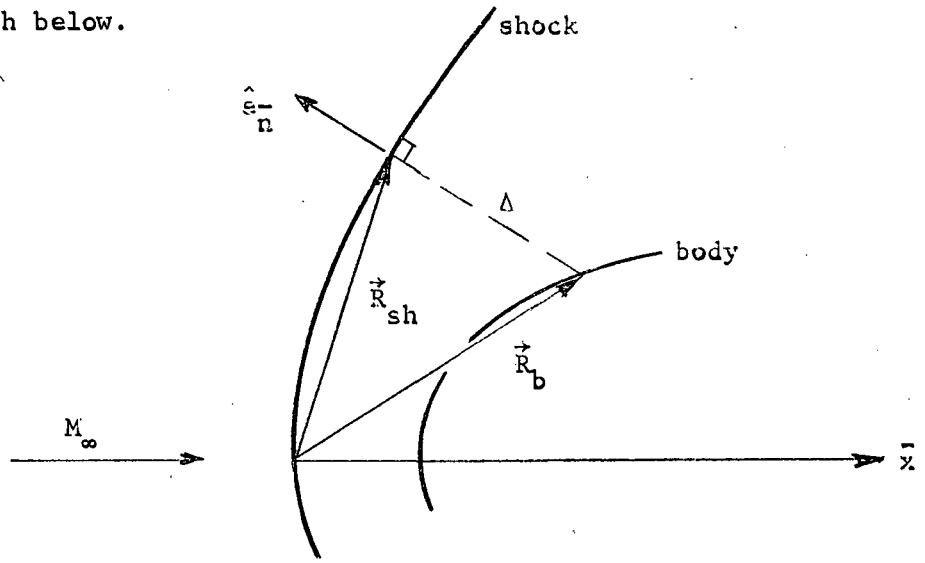

Then, with $\hat{e}_n$ the unit (outer) normal to the shock wave and Δ the stand-off distance, the body point determined by a straight line normal from the shock wave is

$$\vec{R}_b = \vec{R}_s - \Delta\hat{e}_n \qquad \text{(B4)}$$

Let

$$\vec{R}_b = \bar{x}_b\ \hat{e}_{\bar{x}} + \bar{y}_b\ \hat{e}_{\bar{y}} + \bar{z}_b\ \hat{e}_{\bar{z}} \qquad \text{(B5)}$$

$$\vec{R}_s = \bar{x}\,\hat{e}_{\bar{x}} + \bar{y}\,\hat{e}_{\bar{y}} + \bar{z}\,\hat{e}_{\bar{z}} \tag{B6}$$

Now substitute eqs. (B5), (B6), and (3) into (B4). The result gives

$$\bar{y}_b = \bar{y} - \Delta \cos \bar{\Gamma} \cos \bar{\sigma} \tag{B7}$$

$$\bar{z}_b = \bar{z} - \Delta \cos \bar{\Gamma} \sin \bar{\sigma} \tag{B8}$$

Near the stagnation line, eqs. (4) and (5) give

$$\cos \bar{\Gamma} \cos \bar{\sigma} \approx \bar{y}/\bar{R}_{11} \tag{B9}$$

and

$$\cos \bar{\Gamma} \sin \bar{\sigma} \approx \bar{z}/\bar{R}_T \tag{B10}$$

Substitute eqs. (B9) and (B10) into (B7) and (B8) to obtain

$$\bar{y}_b \approx \bar{y}\left(1 - \frac{\Delta}{\bar{R}_{11}}\right) \tag{B11}$$

$$\bar{z}_b \approx \bar{z}\left(1 - \frac{\Delta}{\bar{R}_T}\right) \tag{B12}$$

Now near the stagnation line the body is represented by a portion of an ellipsoid, in a manner similar to the shock wave. Therefore, following the form of eq. (4),

$$\sin^2 \bar{\Gamma}_b = \left(1 + \left(\frac{\bar{y}_b}{\bar{R}_{11,b}}\right)^2 + \left(\frac{\bar{z}_b}{\bar{R}_{T,b}}\right)^2\right)^{-1} \tag{B13}$$

and substituting eqs. (B11) and (B12),

$$\sin^2 \bar{\Gamma}_b = \left(1 + \frac{\bar{y}^2}{\bar{R}_{11,b}^2}\left(1 - \Delta/\bar{R}_{11}\right)^2 + \frac{\bar{z}^2}{\bar{R}_{T,b}^2}\left(1 - \Delta/\bar{R}_T\right)^2\right)^{-1} \tag{B14}$$

Next, substitute eqs. (B14), (45), (49), (21), (24), (43) into eq. (B3) to obtain

$$\begin{aligned}(p_2 - p_\infty)&\left[1 + \frac{\bar{z}^2(1 - \Delta/\bar{R}_T)^2}{R_{T,b}^2} + \frac{\bar{y}^2(1 - \Delta/\bar{R}_{11})^2}{R_{11,b}^2}\right]^{-1} + p_\infty \\ &= p_2 - \Delta p\left[\frac{\bar{z}^2}{\bar{R}_T^2} + \frac{\bar{B}^2\bar{y}^2}{\bar{R}_T^2}\right] - \frac{\left(\frac{\bar{z}^2}{\bar{R}_T^2} + \frac{\bar{B}^3\bar{y}^2}{\bar{R}_T^2}\right)\rho_\infty V_\infty^2}{(\bar{B}+1)\left[1 + \frac{\bar{z}}{\bar{R}_T^2} + \frac{\bar{B}^2\bar{y}^2}{\bar{R}_T^2}\right]}\end{aligned} \tag{B15}$$

Expand this equation and neglect all terms of magnitude higher than $\bar{z}^2$ and/or $\bar{y}^2$. Then the resultant must be independent of $\bar{z}$ and $\bar{y}$; hence, the coefficients of $\bar{z}$ and $\bar{y}$ must each be zero. Equating the coefficients of $\bar{z}^2$ in the resulting equation gives

$$\frac{R_{T,b}^2}{\bar{R}_T^2} = \frac{\left[\frac{p_2 - p_\infty}{\rho_\infty V_\infty^2}\right]\left[1 - \frac{\Delta}{\bar{R}_T}\right]^2}{\frac{\Delta p}{\rho_\infty V_\infty^2} + \frac{1}{\bar{B}+1}} \tag{B16}$$

Similarly, equating the coefficients of $\bar{y}^2$ gives

$$\frac{\bar{B}^2}{B^2} = \frac{\left[1 - \frac{\bar{B}\Delta}{\bar{R}_T}\right]^2\left[\frac{\Delta p}{\rho_\infty V_\infty^2} + \frac{1}{\bar{B}+1}\right]}{\left[1 - \frac{\Delta}{\bar{R}_T}\right]^2\left[\frac{\Delta p}{\rho_\infty V_\infty^2} + \frac{\bar{B}}{\bar{B}+1}\right]} \tag{B17}$$

where

$$B \equiv \frac{R_{T,b}}{R_{11,b}} \tag{B18}$$

In general, eqs. (B17) and (57) must be solved iteratively to find $\Delta/\bar{R}_T$ and $\bar{B}$ for a given value of B and $\Delta p/(\rho_\infty V_\infty^2)$. Then eq. (B16) can be used to calculate $\bar{R}_T$ for a given $R_{T,b}$. Note that for an ideal gas, eq. (A9) gives

$$\frac{\Delta p}{\rho_\infty V_\infty^2} = \frac{2}{\gamma + 1} .$$

APPENDIX C

DESCRIPTION OF COMPUTER PROGRAM CHANGES

This appendix describes the changes necessary to modify the computer program listed in Ref. 3 to include the effects of variable entropy at the edge of the boundary layer. Changes are required for the MAIN program and function RUNGE subprogram in Ref. 3, and two new subroutines SHPROP and SHOFF must be added to the computer program listed in Ref. 3. A description of the additional input and output parameters is also given below.

Main Program

The main program reads part of the input data, calculates the initial data for each streamline on the $\bar{\epsilon}$-circle around the stagnation point, and then calculates and prints the heating rates and other pertinent data along each streamline (independently of the other streamlines). The program variables involved with the changes to the main program are listed below, followed by a listing of the main program.

B: ratio of body principal radii of curvature at stagnation point

BB ratio of shock principal radii of curvature at stagnation line, $\bar{B}$

DOR ratio of shock standoff distance to shock radius of curvature, $\Delta/\bar{R}_T$

F(8) $\sin \bar{\Gamma}\ (\bar{\xi},\bar{\beta})$ for KP = 0

F(9) Ψ_{sh} for KP = 0

F(10) $\sin \bar{\Gamma}\ (\bar{\xi},\bar{\beta})$ for KP > 0

F(11) Ψ_{sh} for KP > 0

GBK local shock angle, $\bar{\Gamma}\ (\bar{\xi},\bar{\beta})$

GBL shock angle where streamline at boundary layer edge crossed the shock, $\bar{\Gamma}\ (\bar{\beta},\Psi)$

G(1,L) Ψ_{sh} at position L along streamline (slug/sec)

G(2,L) shock angle $\bar{\Gamma}\ (\bar{\xi},\bar{\beta})$ at position L along streamline

G(3,L) $D\bar{\Gamma}/D\Psi$ (sec/slug)

HSHK enthalpy aft of local shock angle, h_{sh} (ft^2/sec^2)

KE input parameter; KE = 0 for normal-shock entropy, KE = 2 for variable entropy

NE number of differential equations to integrate minus KE

PB surface pressure for shock solution only, P_b (lb/ft^2)

PSH pressure aft of shock where streamline at boundary layer edge crossed shock, p_{sh} (lb/ft^2)

PSHK pressure aft of shock at edge of local shock layer, p_{sh} (lb/ft^2)

PSS stream function, Ψ (slug/sec)

RHOSHK density aft of shock at edge of local shock layer, ρ_{sh} $(slug/ft^3)$

RPER body radius of curvature, $R_{T,b}$ (ft)

RTB shock radius of curvature, $\bar{R}_T$ (ft)

SPL sine of shock angle where streamline at boundary layer edge crossed shock, sin $\bar{\Gamma}\ (\bar{\beta},\Psi)$

Y(I) $\int_o^s F(I)\ DS$, where I = 1, 2, ..., NR

YB $\bar{y}$

ZB $\bar{z}$

The listing of the main program and the changes in function RUNGE are listed on the following pages. A line drawn through a statement indicates that statement in the original program should be deleted. A rectangle drawn around statements indicates that these are new statements to be added to the program.

```
C          MAIN PROGRAM
      ~~DIMENSION Y(9),F(9),NAM(20)~~
      DIMENSION Y(11),F(11),NAM(20)
      DIMENSION G(3,100)
      COMMON X(20),FN(20,20),RO,XMF(20,20),HX(20),GAM(20,20),AMF(20,20),
     1HP(20),PH(20),PHI(20),FT(20),HPT(20),AMFT(20),AMFF(20),
     2 FNN(20),BMFF(20),XMFF(20),BMF(20,20),DLP(20,20),DLPP(20)
      COMMON/COM3/CAL,SAL,CPH,SPH
      COMMON/COM4/POP,DPDX,DPXX,DPXP,DPDP,DP2P
      COMMON/COM5/F2,FX,FXX,FP,FPP
      COMMON/COM6/PIN,VIN,RHOIN,EMIN,HS
      INTEGER RUNGE
      PI=3.1415927
      READ(1,1000) NAM
 1000 FORMAT(20A3)
      WRITE(3,1001) NAM
 1001 FORMAT(2X,20A3)
      CALL BGEOM(IMAX,KMAX)
      READ(1,900)PIN,TIN,VIN,TRI,TRE,CST,HMAX,KG,KTR,KS,NMAX,KPO
     1,KE
  ~~900 FORMAT(7E10.0/5I10)~~
  900 FORMAT(7E10.0/6I10)
      IF(KTR.EQ.-1)CALL TRANS
C    KG=0 FOR PERF. GAS, KG=1 FOR EQUIL. AIR,  KTR=-1 FOR TRANSITION
C    BASED ON GEOM. LOC., KTR=0 FOR R.N.(MOM THK), KTR=1 FOR INTEGR. UNIT
C    R.N.,  TRI=BEG. OF TRANSITION,  TRE=END OF TRANSITION,  CST CONVERTS
C    BODY UNITS TO FT., KS=0 FOR STREAMLINES ONLY, KPO=1 FOR ADD'L PRINT
C    KE=0 CONST ENTROPY AT EDGE OF B.L., KE=2 FOR VARIABLE ENTROPY
C  COMPUTE BODY GEOMETRY
      READ(1,2)ALPD,ZW,KBM,KP
    2 FORMAT(2F10.5,2I5)
      ALP=ALPD*PI/180.
      SAL=SIN(ALP)
      CAL =COS(ALP)
C  KP=0 FOR SIMPLIFIED STRMLNS, KP=1 FOR NEWP, KP=2 FOR INPUT PRESSURES
C  COMPUTE STAGNATION POINT XO,GIVEN AN ANGLE OF ATTACK,ALP
      CALL STAGN(ALP,IMAX,KMAX,XO,RPER,B,ISTG)
```

```
C  ISTG IS AN INDICATOR VARIABLE
C       IF ISTG=-1 => NEGATIVE ANGLE OF ATTACK
C       IF ISTG=0 => STAGNATION POINT NOT FOUND
C       IF ISTG=1 => STAGNATION POINT FOUND
       CALL STGPR(PIN,TIN,VIN,RHOIN,EMIN,PS,RHOS,HS,KG)
       WRITE(3,1002)PIN,TIN,RHOIN,VIN,EMIN
 1002 FORMAT(//,47X,22HFREE STREAM PROPERTIES,//,1X,18HPRESSURE(LB/SQ FT
     1),10X,11HTEMP(DEG R),10X,20HDENSITY(SLUGS/CU FT),10X,16HVELOCITY(F
     2T/SEC),10X,8HMACH NO.,//
     4,3X,E14.6,11X,E14.6,11X,E14.6,14X,E14.6,9X,E14.6//)
       WRITE(3,1009)PS,RHOS,HS
 1009 FORMAT(//,44X,21HSTAGNATION PROPERTIES,//,10X,18HPRESSURE(LB/SQ FT
     1),10X,20HDENSITY(SLUGS/CU FT),10X,22HENTHALPY(SQ FT/SQ SEC),//
     3,12X,E14.6,15X,E14.6,17X,E14.6/)
      ~~WRITE(3,1007)TRI,TRE,CST,KG,KTR,KP,HMAX,NMAX,KPO,KS,IMAX,KMAX~~
      WRITE(3,1007)TRI,TRE,CST,KG,KTR,KP,HMAX,NMAX,KPO,KS,IMAX,KMAX,KE
 1007 FORMAT(//,12X,5HTRI =,E14.6,10X,5HTRE =,E14.6,10X,5HCST =,E14.6,//
     1,12X,4HKG =,I10,15X,5HKTR =,I10,14X,4HKP =,I10
     2,//,12X,6HHMAX =,E14.6, 9X,6HNMAX =,I10,13X,5HKPO =,I10//
     ~~3,12X,4HKS =,I10,15X,6HIMAX =,I10,13X,6HKMAX =,I10//)~~
     3,12X,4HKS =,I10,15X,6HIMAX =,I10,13X,6HKMAX =,I10,//,12X,4HKE =
     4,I10/)
       CALL SHPROP(1.,P2,RHO2,H2,KG)
       WRITE(3,1011)P2,RHO2,H2
 1011 FORMAT(5X,'P2 =',E12.5,4X,'RHO2 =',E12.5,4X,'H2 =',E12.5,//)
       CALL SHOFF(B,RPER,P2,RHO2,H2,BB,RTB,DOR,KG)
       PNEWT=1.-PIN/PS
       CALL PRESS(KP,PNEWT)
       HW=ZW*HS
       TW=HW/6006.
       VISW=2.27E-08*TW**1.5/(TW+198.6)
       RHOSW=PS/(TW*1716.)
       CALL PROP(PS,HS,RHOS,PS,HE,RHOE,UE,VISS,EMS,KG)
       DUEDPS=SQRT(2.*(PS-PIN)/RHOS)/VIN
       CTHM1=2.*PS*VISW*VIN/(1716.*TW)
       CTHM=0.4696*SQRT(CTHM1/CST)
C    DUEDPS=D(UE/VIN)/D(PSI),  CTHM=CONST. FOR MOM. THK.
```

```
      IF(ISTG)28,30,33
   28 WRITE(3,29)
   29 FORMAT(/,2X,40H*** NEGATIVE ANGLE OF ATTACK ENCOUNTERED,/,6X,42HSTA
     1AG. POINT SET TO 0.0, PROGRAM CONTINUING)
   33 WRITE(3,21)ALPD,ZW,KBM
   21 FORMAT(///,2X,23HSTREAMLINE CALCULATIONS,//,5X,11HINPUT DATA:,/,5X
     1,16HANG. OF ATTACK= E12.5,2X,4HDEG.,/,5X,12HZETA(WALL)= E12.5,/,5X
     2,36HNO. OF STREAMLINES TO BE CALCULATED=,I3)
      KB=1
C  KBM IS MAX NO OF BETAS READ IN, KB.LT.KBM
      IF(ALP.NE.0.) CALL STRMLN(XO,0.,DLPH,DDP,DDX,GM,DGP,DGX,FFO,IMAX,
     1KMAX)
      IF(ALP.EQ.0.)FFO=0.
      WRITE(3,15)B,XO
   15 FORMAT(///,5X,2HB=E12.5,/,5X,20HSTAGNATION POINT,XO=E12.5)
      IF(B.GE.1.)BBARS=1./(B+1.)
      IF(B.LT.1.)BBARS=B/(B+1.)
C  BBARS IS B.L. BETA AT STAG. PT.
      BEXP=BBARS**.686
      G7=(1.116+.411*BEXP)/(1.+.527*BEXP)
      AS=.1-.08*(BBARS-.5)
      BS=.5-AS
      QQ1=SQRT((B+1.)*DUEDPS*VIN/(RPER*CST))
C    QWS=STAG. PT. H. T. IN BTU/(FT*FT*SEC)
      ZONK=.892E-03
      QWS=ZONK*QQ1*(RHOSW*VISW)**AS*(RHOS*VISS)**BS*(HS-HW)/G7
      QWSB=QWS/(HS-HW)
      HSP=QWSB*6006.
      WRITE(3,1003)TW,QWS,HSP
 1003 FORMAT(//, 5X,4HTW =,E14.6,6H DEG R,10X,5HQWS =,E14.6
     1,14H BTU/SQ FT-SEC,10X,5HHSP =,E14.6,20H BTU/SQ FT-SEC-DEG R,/)
      G5=SQRT(DUEDPS*2.*(B+1.)/RPER)
      PORV=PS/(RHOS*VIN**2)
      DEPS=0.1*RPER
    3 READ(1,4)BETAD
    4 FORMAT(F10.5)
      WFN=0.
```

```
      HC=0
      BETA=BETAD*PI/180.
      L1=1
      L2=1
      MR=0
      STR=0.
      NT=1
      NR=5
      NE=5
      IF(KP.GE.1)NR=7
      IF(KP.GE.1)NE=7
      NR=NE+KE
      F(NE+1)=0
      F(NE+2)=1
      IF(KS.EQ.0)NT=3
      NCS=1
      DS = 0.1*DEPS
      WRITE(3,41)KB,BETAD
   41 FORMAT(//,2X,18HFOR STREAMLINE NO.I2,12H WHERE BETA=E12.5,3HDEG,/,
     12X,32HTHE CALCULATIONS ARE AS FOLLOWS:)
      WRITE(3,42)
   42 FORMAT(//,13X,1HX,13X,1HY,14X,1HZ,14X,1HH,14X,1HS,13X,4HBBAR
     1,10X,4HP/PS,8X,6HQW/QWS)
      IF(KPO.EQ.1)WRITE(3,1005)
 1005 FORMAT(13X,2HUE,12X,2HHE,11X,4HRHOE,11X,3HMUE,11X,7HMACH NO,10X
     1,5HRN/FT,9X,7HMOM.THK,6X,3HRNM,/,12X,3HRN1,13X,1HR,12X,3HPHI,11X
     2,7HDR/DPHI,7X,9HD2R/DPHI2,8X,5HDR/DX,9X,7HD2R/DX2,5X,6HQB/QSB,/)
      IF(KE.EQ.2)WRITE(3,1012)
 1012 FORMAT(12X,3HGBK,11X,3HGBL,12X,3HPSH,12X,4HPSHK,12X,2HPB,13X,2HPE,
     110X,8HPSS(SHK),9X,3HPSS)
C  Y(1)=XX,  Y(2)=PPH,  Y(3)=H
C  F(1)=DX/DS,  F(2)=D(PHI)/DS,  F(3)=DH/DS
C  F(4)=(POP)(UDU)(H)**2,  F(5)=(RHOE)(UE)(CST)/VISC
      CBE=COS(BETA)
      SBE=SIN(BETA)
      CB4=B*CBE**2+SBE**2
      CB5=(B*CBE)**2+SBE**2
```

```
~~Y(1)=XO+DEPS*(CBE*SAL+CAL*DEPS*CB4/2./RPER)~~
~~ZZ=DEPS*SBE~~
~~YY=FFO+DEPS*(CBE*CAL-SAL*DEPS*CB4/2./RPER)~~
      YB=DEPS*CBE/SQRT(CB4)
      ZB=DEPS*SBE/SQRT(CB4)
      Y(1)=XO+YB*SAL+DEPS**2*CAL/RPER/2
      YY=FFO+YB*CAL-DEPS**2*SAL/RPER/2
      ZZ=ZB
      IF(ABS(YY).LT.(1.E-05*ZZ))Y(2)=PI/2.
      IF(ABS(YY).GE.(1.E-05*ZZ))Y(2)=ATAN(ZZ/YY)
      IF(Y(2).LT.0.)Y(2)=PI+Y(2)
      IF(BETAD.EQ.0.)Y(2)=0.
~~Y(3)=DEPS*CB4/SQRT(CB5)~~
~~Y(4)=DUEDPS*CB4**2*DEPS**4/RPER/(2.*B+2.)~~
      Y(3)=DEPS/CB4*SQRT(CB5/CB4)
      Y(4)=DUEDPS/RPER*CB5**2*(DEPS/CB4)**4/2/(B+1)
      CALL STRMLN(Y(1),Y(2),DLPH,DDP,DDX,GM,DGP,DGX,FF,IMAX,KMAX)
      SGM=SIN(GM)
      CGM=COS(GM)
      TN=-SAL*SIN(DLPH-Y(2))
      TD=CAL*CGM-SAL*SGM*COS(DLPH-Y(2))
      IF(ABS(TD).LT.(1.E-05*ABS(TN)))Y(5)=PI/2.
      IF(ABS(TD).GE.(1.E-05*ABS(TN)))Y(5)=ATAN(TN/TD)
      IF(Y(5).LT.0.)Y(5)=PI+Y(5)
~~Y(6)=B*(CB4/CB5)**2~~
      IF(BETAD.EQ.0.)Y(5)=0.
      Y(6)=B/CB5
      Y(NE)=RHOS/VISS*CST/2/RPER*DUEDPS*DEPS**2
      ZR2=(ZB/(1-DOR)/RTB)**2
      YR2=(YB*BB/(1-DOR*BB)/RTB)**2
      Y(NE+1)=1/SQRT(1+ZR2+YR2)
      Y(NE+2)=RHOIN*VIN*CB5/(B+1)*(DEPS/CB4)**2
      L=0
      EXET=2.*(B-1.)
      IF(B.LT.1.)EXET=2*(1./B-1.)
      AS1=SBE**2
      IF(B.LT.1.)AS1=CBE**2
```

```
      BS1=(1.-AS1**2)*B**2
      IF(B.LT.1.)BS1=BS1/B**4
      SUM=0.
      DO 90 MQ=1,9,2
      AMQ=MQ
      SUM=SUM+4.*SQRT(AS1+BS1*(.1*AMQ)**EXET)
      IF(MQ.EQ.9)GO TO 91
   90 SUM=SUM+2.*SQRT(AS1+BS1*(.1*(AMQ+1.))**EXET)
   91 S=DEPS*.1/3.*(SQRT(AS1)+SQRT(AS1+BS1)+SUM)
      S=S/SQRT(CB4)
      PSS=0
      Y(NR)=DUEDPS*(DEPS*CB4)**2*CST*RHOS/2./RPER/VISS
      K=0
      IF(KP.EQ.0)GO TO 22
      IF(KP.GE.1)GO TO 71
    5 K=RUNGE(Y,F,S,DS,NR,HMAX,MR)
      IF(K.EQ.2)GO TO 310
      IF(Y(3).LE.1.E-04)GO TO 74
   22 CALL STRMLN(Y(1),Y(2),DLPH,DDP,DDX,GM,DGP,DGX,FF,IMAX,KMAX)
C  CPSI=COS(PSI),  SPSI=SIN(PSI),  STH=SIN(THETA),  CTH=COS(THETA)
C  DGB=D(GM)/(H*D(BETA)),  -DSB=D(SIG)/(H*D(BETA))
      SGM=SIN(GM)
      CGM=COS(GM)
      CPSI=CAL*SGM+SAL*CGM*COS(DLPH-Y(2))
      SPSI=SQRT(1.-CPSI*CPSI)
      STH=SAL*SIN(Y(2)-DLPH)/SPSI
      F(1)=(CAL-CPSI*SGM)/SPSI
      CTH=F(1)/CGM
      IF(ABS(CTH).LT.1.E-05)THE=PI/2.
      IF(ABS(CTH).GE.1.E-05)THE = ATAN(STH/CTH)
      IF(THE.LT.0.)THE=PI+THE
      F(2)=(STH*COS(DLPH)-CTH*SIN(DLPH)*SGM)/FF
      IF(Y(2).LE.0.0.OR.Y(2).GE.PI)F(2)=0.
      AA1=-STH*CGM
      AA2=(CTH*COS(DLPH)+STH*SIN(DLPH)*SGM)/FF
      DGB=AA1*DGX+AA2*DGP
      DSB=AA1*DDX+AA2*(DDP-1.)
```

```
      F(3)=Y(3)*CPSI/SPSI*(STH*DGB-CTH*CGM*DSB)
      POP=PNEWT*CPSI*(CPSI+ABS(CPSI))/2.+1.-PNEWT
      PE=POP*PS
      IF(KE.EQ.2)GO TO 425
      CALL PROP(PS,HS,RHOS,PE,HE,RHOE,UE,VISC,EM2,KG)
      EM=SQRT(EM2)
      THM=CTHM*SQRT(Y(4))/(UE*Y(3)*RHOE)
  423 EM=SQRT(EM2)
      DGS=F(1)*DGX+F(2)*DGP
      DSS=F(1)*DDX+F(2)*(DDP-1.)
      DPSIS=-CTH*DGS-CGM*STH*DSS
      UOU=UE/VIN
      ROR=RHOE/RHOS
      PUH=POP*UOU*Y(3)
      BIFF=.5*(CPSI+ABS(CPSI))
      DPS=-2.*PNEWT*BIFF*SPSI*DPSIS
      DUEDS=-PORV*DPS/ROR/UOU
      F(4)=PUH*Y(3)
      F(5)=RHOE*UE/VISC*CST
      RNF=F(5)/CST
      RN1=Y(5)
      THM=CTHM*SQRT(Y(4))/(UE*Y(3)*RHOE)
      RNM=F(5)*THM
      IF(KE.EQ.0)GO TO 426
      PB=PIN+(PE-PIN)*(P2-PIN)/(PS-PIN)
      CALL SHPROP(Y(6),PSHK,RHOSHK,HSHK,KG)
      F(6)=Y(3)*(PB-PSHK)/Y(7)/VIN
      F(7)=Y(6)*Y(3)*RHOIN*VIN
      GO TO (74,80),L1
  426 GO TO (74,80),L1
   74 CONTINUE
      IF(K.EQ.1)GO TO 5
    6 L=L+1
      IF(Y(3).LE.1.E-04)GO TO 312
      IF(RNM.LE.1.E-04)GO TO 314
C   DGS=D(GM)/DS, -DSS=D(SIG)/DS,  DPSIS=D(PSI)/DS
C   BBAR=B.L.BETA,  ZW=H(W)/H(E),  ZWP=ZETA(W)'/ZETA(W,S)'
```

```
C  FROM NASA TR R-118
   62 TE=HE/HS
      BBAR=Y(4)*2.*DUEDS/(TE*PUH*UOU*Y(3))
      IF (DPS.GT.0.) BBAR = 0.
   63 AA4 = BBAR**.686
      AA5=(1.+.527*AA4)/(1.116+.411*AA4)
      AA6=1.1-.1625*TE+.0625*TE*TE
      AA7=(.85+.15*TE-ZW)/(1.-ZW)
      ZWP=G7*AA5*AA6*AA7
      QOQS=PUH*ZWP/SQRT(Y(4))/G5
      QOQSB=QOQS/AA7
      QWL=QOQS*QWS
      QWLB=QOQSB*QWSB
      YY=FF*COS(Y(2))
      ZZ=FF*SIN(Y(2))
      THMF=THM*CST
      PHID=Y(2)*180./PI
      GO TO (75,76,73),NT
   73 QW=QWL
    7 WRITE(3,17)Y(1),YY,ZZ,Y(3),S,BBAR,POP,QOQS
   17 FORMAT(2X,8(3X,E12.5))
      IF(KPO.EQ.1)WRITE(3,1008)UE,HE,RHOE,VISC,EM,RNF,THMF,RNM,RN1,FF
     1,PHID,FP,FPP,FX,FXX,QOQSB
 1008 FORMAT(3X,8(3X,E12.5),/,4X,8(3X,E12.5),/)
      IF(KE.EQ.2)WRITE(3,1010)GBK,GBL,PSH,PSHK,PB,PE,Y(NE+2),PSS
 1010 FORMAT(5X,8(3X,E12.5))
      IF(BETAD.GE.180..AND.Y(1).LT.(1.E-04*X(2)))GO TO 50
      IF(L-NMAX)8,8,9
    8 IF(Y(1).LT.X(IMAX).AND.KP.EQ.0) GO TO 5
      IF(Y(1).LT.X(IMAX).AND.KP.GE.1) GO TO 70
      WRITE(3,14)BETAD,L
   14 FORMAT(/,2X,26H*** CALCULATIONS FOR BETA=E12.5,15H HAS TERMINATED,
     1/,5X,5HAFTER I3,16H INTEGRATIONS **)
   19 IF(KB.GE.KBM)GO TO 10
      KB=KB+1
      GO TO 3
    9 WRITE(3,18) KB
```

```
   18 FORMAT(/,2X,30H*** SUBSCRIPT OUT OF RANGE ***,/,6X,32HCALCULATIONS
     1 FOR STREAMLINE NO. ,I2,13H DISCONTINUED)
        GO TO 19
   10 WRITE(3,101) KB
  101 FORMAT(/,2X,20HTHE CALCULATIONS FOR,I3,31H STREAMLINES HAS BEEN CO
     1MPLETED,/,2X,19HPROGRAM TERMINATING)
        GO TO 32
  310 WRITE(3,311) KB,DS
  311 FORMAT(/,2X,25HINTEGRATION OF STREAMLINE,I2,30H DISCONTINUED DUE T
     1O STEP SIZE,/,5X,6H*** H=E12.5,4H ***)
        GO TO 19
  312 WRITE(3,313)Y(3),KB
  313 FORMAT(/,2X,33HSCALE FACTOR (H) GOING NEG ,***H=E12.5,/,2X,
     1110HSTREAMLINE(3,12HDISCONTINUED)
        GO TO 19
  314 WRITE(3,315)RNM,KB
  315 FORMAT(/,2X,31HREY NO (RNM) GOING NEG,*** RNM=E12.5,/,2X
     1,10HSTREAMLINE(3,12HDISCONTINUED)
        GO TO 19
   30 WRITE(3,31)
   31 FORMAT(/,2X,43H*** STAGNATION POINT NOT FOUND, RUN ABORTED)
        GO TO 32
C  NOSE REGION FOR BETA=PI
   50 Y(2)=PI
      IF(KP.GE.1)Y(5)=0.
        GO TO 8
C  ROUTINE FOR NEWP OR INPUT PRESSURES
   70 K=RUNGE(Y,F,S,DS,NR,HMAX,MR)
        IF (K.EQ.2) GO TO 310
        IF(Y(3).LE.1.E-04)GO TO 72
   71 CALL STRMLN(Y(1),Y(2),DLPH,DDP,DDX,GM,DGP,DGX,FF,IMAX,KMAX)
        THE=Y(5)
        SPH = SIN(Y(2))
        CPH = COS(Y(2))
        SGM = SIN(GM)
        CGM = COS(GM)
        STH = SIN(Y(5))
```

```
      CTH = COS(Y(5))
      SDLP = SIN(DLPH)
      CDLP = COS(DLPH)
      F(1) = CTH*CGM
      F(2) = (STH*CDLP-CTH*SDLP*SGM)/FF
      IF(Y(2).LE.0.0.OR.Y(2).GE.PI)F(2)=0.
      F(3) = Y(6)
      CALL PDER(Y(1),Y(2),POP,DPDP,DP2P,DPDX,DPXP,DPXX)
      PE=PS*POP
      IF(KE.EQ.2)GO TO 425
      CALL PROP(PS,HS,RHOS,PE,HE,RHOE,UE,VISC,EM2,KG)
      THM=CTHM*SQRT(Y(4))/(UE*Y(3)*RHOE)
  424 EM=SQRT(EM2)
      UOU=UE/VIN
      PUH=POP*UOU*Y(3)
      F(4) = PUH*Y(3)
      ROR=RHOE/RHOS
      DSS = F(1)*DDX+F(2)*(DDP-1.)
      DXB = -STH*CGM
      DPHB = (CTH*CDLP+STH*SDLP*SGM)/FF
      DPB = DXB*DPDX+DPHB*DPDP
      UESQ=UOU**2
      F(5)=-DPB*PORV/UESQ/ROR+SGM*DSS
      IF(Y(2).LE.0.0.OR.Y(2).GE.PI)F(5)=0.
C  F(5) = D(THETA)/DS, F(6) = D2H/D(S**2)
      HT1=CGM**2*CDLP*(DDX*DGP-DGX*(DDP-1.))/FF
      HT2=(DPB*PORV/UESQ/ROR)**2*(3.-EM2)
      DSB = DXB*DDX+DPHB*(DDP-1.)
      DTHB = Y(6)/Y(3)+SGM*DSB
      DPS = F(1)*DPDX+F(2)*DPDP
      DGB = DXB*DGX+DPHB*DGP
      DDLB = DXB*DDX+DPHB*DDP
      HT3=-CTH*SDLP+STH*CDLP*SGM
      HT4 = DPDX*STH*SGM*DGB
      HT5=DPDP/FF*(STH*SDLP*CGM*DGB+HT3*(DDLB+DPHB*FF))
      HT6= STH*CGM*(STH*CGM*DPXX-DPHB*DPXP)
      HT7= DPHB*(-STH*CGM*DPXP+DPHB*DP2P)
```

```
      D2PB = -DTHB*DPS+HT4+HT5+HT6+HT7
      F(6)=Y(3)*(-D2PB*PORV/UESQ/ROR-HT2+HT1)
      F(7)=RHOE*UE/VISC*CST
      RNF=F(7)/CST
      RN1=Y(7)
      THM=CTHM*SQRT(Y(4))/(UE*Y(3)*RHOE)
      RNM=F(7)*THM
      DUEDS=-PORV*DPS/(ROR*UOU)
      IF(KE.EQ.0)GO TO 427
      PB=PIN+(PE-PIN)*(P2-PIN)/(PS-PIN)
      CALL SHPROP(Y(8),PSHK,RHOSHK,HSHK,KG)
      F(8)=Y(3)*(PB-PSHK)/Y(9)/VIN
      F(9)=Y(8)*Y(3)*RHOIN*VIN
  427 GO TO (72,80),L1
      GO TO (72,80),L1
   72 CONTINUE
      IF (K .EQ. 1 ) GO TO 70
      IF(Y(3).LE.1.E-04)GO TO 312
      IF(RNM.LE.1.E-04)GO TO 314
      L = L+1
      GO TO 62
   75 STRL=STR
      STR=Y(1)
      TRIL=TRI
      TREL=TRE
      IF(KTR.EQ.0)STR=RNM
      IF(KTR.EQ.1)STR=RN1
      GO TO (81,82,83,84),L2
   81 IF(KTR.EQ.-1)CALL BEGTR(Y(2),TRI)
      IF(STR.LT.TRI)GO TO 73
      DS=DS*(TRIL-STRL)/(STR-STRL-TRI+TRIL)
      MR=1
      L2=2
      GO TO 8
   82 NR=NR+2
      MR=0
      L1=2
```

```
      L2=3
      Y(NR-1)=THM
      HC=1.2168/.4696
      HTR=(HC-UE**2/2./HE)*HE/HS
      HI=HTR-(HW/HS-1.)*1.3
      Y(NR)=HI
      WRITE(3,1004)
 1004 FORMAT(/,10X,31H****BEGINNING OF TRANSITION****/)
      WRITE(3,17)Y(1),YY,ZZ,Y(3),S,BBAR,POP,QOQS
      IF(KPO.EQ.1)WRITE(3,1008)UE,HE,RHOE,VISC,EM,RNF,THMF,RNM,RN1,FF
     1,PHID,FP,FPP,FX,FXX,QOQSB
      IF(KE.EQ.2)WRITE(3,1010)GBK,GBL,PSH,PSHK,PB,PE,Y(NE+2),PSS
      K=1
      DS=DS/30.
      GO TO 80
   83 IF(KTR.EQ.-1)CALL ENDTR(Y(2),TRE)
      IF(STR.GE.TRE)GO TO 85
      NCS=0
      XI=4.74*(STR-TRI)/(TRE-TRI)
      EXW=EXP(-.412*XI**2)
      WFN=1.-EXW
      QW=QWL+WFN*(QWT-QWL)
      QWB=QWLB+WFN*(QWTB-QWLB)
      QOQS=QW/QWS
      QOQSB=QWB/QWSB
      GO TO 7
   85 DS=DS*(TREL-STRL)/(STR-STRL-TRE+TREL)
      WFN=1.
      MR=1
      L2=4
      GO TO 8
   84 MR=0
      NT=2
      QOQS=QWT/QWS
      QOQSB=QWTB/QWSB
      QW=QWT
      WRITE(3,17)Y(1),YY,ZZ,Y(3),S,BBAR,POP,QOQS
```

```
      IF(KPO.EQ.1)WRITE(3,1008)UE,HE,RHOE,VISC,EM,RNF,THMF,RNM,RN1,FF
     1,PHID,FP,FPP,FX,FXX,QOOSB
      IF(KE.EQ.2)WRITE(3,1010)GBK,GBL,PSH,PSHK,PB,PE,Y(NE+2),PSS
      WRITE(3,1006)
 1006 FORMAT(/,10X,25H****END OF TRANSITION****/)
      GO TO 8
   76 QW=QWT
      QOOS=QWT/QWS
      QOOSB=QWTB/QWSB
      GO TO 7
   80 RNM=F(NR-2)*Y(NR-1)
   80 RNM=F(NE)*Y(NR-1)
      IF(RNM.LE.1.E-04)GO TO 86
      THM=Y(NR-1)
      CALL SPCH(ZW,HE,RHOE,UE,HS,RNM,CF,QWT,QWTB,NCS)
      HC=HS/HE*(Y(NR)+(HW/HS-1.)*1.3)+UE**2/2./HE
      F(NR-1)=(EM2-2.-HC)*Y(NR-1)*DUEDS/UOU+CF/2.-Y(NR-1)*F(3)/Y(3)
      W1=Y(NR)+1.
      W2=Y(NR)-1.
      W3=W1*W2
      W4=HW/HS-1.
      W5=W4*(2.6*W2-.15*W1**2/4.3)
      W6=Y(NR)*W1/2.*DUEDS/UOU*HS/HE
      W7=.03*Y(NR)*W3*CF/2./Y(NR-1)
      F(NR)=-W6*(W3+W5)-W7
   86 IF(KP.EQ.0)GO TO 74
      IF(KP.GE.1)GO TO 72
  425 G(1,L)=Y(NE+2)
      DO 430 LBJ=1,5
      IF(PSS.GT.G(1,1))GO TO 428
      Q1=ZR2*(PSS/G(1,1))**(2/(BB+1))
      Q2=YR2*(PSS/G(1,1))**(2*BB/(BB+1))
      SPL=1/SQRT(1+Q1+Q2)
      GO TO 429
  428 CONTINUE
      DO 421 NN=2,L
      IF(PSS.LT.G(1,NN))GO TO 422
```

```
  421 CONTINUE
      PSS=G(1,L)
      SPL=Y(NE+1)
      GO TO 429
  422 N=NN-1
      DEPSS=PSS-G(1,N)
      SPL=G(2,N)+DEPSS*G(3,N)
  429 CALL SHPROP(SPL,PSH,RHOSH,HSH,KG)
      CALL PROP(PSH,HSH,RHOSH,PE,HE,RHOE,UE,VISC,EM2,KG)
      THM=CTHM*SQRT(Y(4))/(UE*Y(3)*RHOE)
      Q4=5.27*THM*(1-WFN)
      Q5=WFN*Y(NR-1)*(10.3-HC)
  430 PSS=RHOE*UE*Y(3)*(Q4+Q5)
      GBK=ARSIN(Y(NE+1))*180./PI
      GBL=ARSIN(SPL)*180./PI
      IF(KP.EQ.0)GO TO 423
      GO TO 424
   32 CALL EXIT
      END
C
C
C
C
      FUNCTION RUNGE(Y,F,X,H,N,HMAX,MR)
      INTEGER RUNGE
      DIMENSION PHI(9),SAVEY(9),Y1(9),Y2(9),YKP(9),FKP(9),Y(N),F(N)
      DIMENSION PHI(11),SAVEY(11),Y1(11),Y2(11),YKP(11),FKP(11),Y(N),F(N
     1)
C       REMAINING PART OF RUNGE IS UNCHANGED
```

Subroutine SHPROP

This subroutine calculates the fluid properties aft of an oblique shock wave for a perfect gas or equilibrium air. A call to subroutine SHPROP has the form

CALL SHPROP (SG, PSH, RHOSH, HSH, KG)

where the arguments are

SG	sine of the shock angle (sin $\bar{\Gamma}$)
PSH	pressure aft of shock, p_{sh} (lb/ft^2)
RHOSH	density aft of shock, ρ_{sh} ($slug/ft^3$)
HSH	enthalpy aft of shock, h_{sh} (ft^2/sec^2)
KG	indicator variable; KG = 0 for perfect gas, KG = 1 for equilibrium air

Other program variables are defined in Ref. 3. A listing of subroutine SHPROP appears on the following page.

```
      SUBROUTINE SHPROP(SG,PSH,RHOSH,HSH,KG)
      COMMON/COM6/PIN,VIN,RHOIN,EMIN,HS
      IF(KG.EQ.0)GO TO 4
      A1=RHOIN*VIN*SG
      A2=PIN+A1*VIN*SG
      A4=HS+VIN**2*(SG**2-1.)/2
      VO=0
      DO 2 J=1,20
      PSH=A2-A1*VO
      IF(PSH.LE.0.)PSH=A2
      HSH=A4-VO**2/2
      IF(HSH.LE.0.)HSH=A4
      PR=(PSH/2117)**.965
      HR=(HSH/2.119E08)**.6123
      DEN=1-1.0477*(1-HR)
      RHOSH=.0294*.002498*PR/DEN
      VSH=A1/RHOSH
      WRITE(3,5)J,PSH,HSH,RHOSH,VO,VSH
    5 FORMAT(6X,'J =',I3,5(3X,E12.5))
      IF(ABS((VSH-VO)/VSH).LT.1.E-05)GO TO 3
    2 VO=VSH
    3 RETURN
    4 A3=(EMIN*SG)**2
      PSH=(7*A3-1)/6 *PIN
      RHOSH=6*A3/(A3+5)*RHOIN
      HSH=(VIN/EMIN)**2/.4*(7*A3-1)*(A3+5)/36/A3
      RETURN
      END
```

Subroutine SHOFF

This subroutine calculates the shock standoff distance at the stagnation line and also the shock principal radii of curvature from the body radii of curvature at the stagnation point. A call to subroutine SHOFF has the form

CALL SHOFF (B, RPER, P2, RHO2, H2, BB, RTB, DOR, KG)

where the arguments are

B	ratio of body principal radii of curvature
RPER	$R_{T,b}$ (body radius of curvature)
P2	pressure aft of normal shock, p_2 (lb/ft^2)
RHO2	density aft of normal shock, ρ_2 ($slug/ft^3$)
H2	enthalpy aft of normal shock, h_2 (ft^2/sec^2)
BB	ratio of shock principal radii of curvature, $\bar{B}$
RTB	shock radius of curvature, $\bar{R}_T$
DOR	ratio of shock standoff distance to shock radius of curvature, $\Delta/\bar{R}_T$
KG	indicator variable; KG = 0 for perfect gas, KG = 1 for equilibrium air

Other program variables are:

DHRP	$\rho_2 \Delta h/\Delta p$
DP	$\Delta p/(\rho_\infty V_\infty^2)$
DRP	$\rho_\infty^2 V_\infty^2 (\partial(1/\rho)/\partial p)_2$
DRH	$\rho_\infty V_\infty^2 (\partial(1/\rho)/\partial h_e)_2$
ROR	ρ_∞/ρ_2

E E (see eq. (A 10))

EMIN freestream Mach number, M_∞

A listing of subroutine SHOFF appears on the the following pages.

```
      SUBROUTINE SHOFF(B,RPER,P2,RHO2,H2,BB,RTB,DOR,KG)
      COMMON/COM6/PIN,VIN,RHOIN,EMIN,HS
      BB=B
      RTB=RPER
      DELP=(P2-PIN)/RHOIN/VIN**2
      ROR=RHOIN/RHO2
      IF(KG.EQ.0)GO TO 1
      PR=(P2/2117)**.965
      HR=(H2/2.119E08)**.6123
      POR=P2/RHOIN/VIN**2
      DRP=-.965*ROR/POR
      DRH=RHOIN*VIN**2*1.0477*.6123*HR/H2/PR/7.344E-05
      DN=1+DRP+ROR*DRH
      UP=-1+.5*DRH*(1-ROR)
      DP=(ROR-1)*UP/DN
      DHRP=(-.5*(1+ROR)*(1+DRP)+ROR*DRP)/UP/ROR
      E=DHRP-1
      GO TO 2
    1 DP=2/(1.4+1)
      EM2=EMIN**2
      E=(EM2-1)**2/2/EM2/(1+.2*EM2)
    2 CROR=ROR/DP/2
      DO 3 I=1,20
      D=1/DP/(BB+1)
      IF(BB.LT.1)D=D*BB
      EX=2/(BB+1)
      IF(BB.LT.1)EX=EX*BB
      AIN=1/SQRT(1+D)/48.
      DO 4 J=1,15,2
      DO 4 K=1,2
      X=(J+K-1)/16.
      DIN=1/SQRT(1+D-D*X+E*X**EX)/48.
      II=2+(2-K)*2
    4 AIN=AIN+II*DIN
      AIN=AIN-DIN
      DOR=SQRT(CROR)/(BB+1)*AIN
      IF(BB.LT.1)DOR=DOR*BB
```

```
      T1=1/(BB+1)
      T2=BB*T1
      T3=DP+T1
      T4=DP+T2
      T5=1-DOR
      T6=1-DOR*BB
      B2=BB
      BB=B*T6/T5*SQRT(T3/T4)
      ER2=ABS((BB-B2)/B2)
      IF(ER2.LT.1.E-04)GO TO 5
    3 CONTINUE
    5 RTB=RPER*SQRT(T3/DELP)/T5
      WRITE(3,6)B,BB,RPER,RTB,DOR,I
    6 FORMAT(//,4X,3HB =,E12.5,4X,4HBB =,E12.5,4X,6HRPER =,E12.5,4X
     1,5HRTB =,E12.5,//,4X,5HDOR =,E12.5,4X,12HNO.OF ITER =,I3,/)
      RETURN
      END
```

Description of New Input Parameter

Only one additional input parameter is required, KE. The read statement, near the beginning of the main program, corresponding to format statement number 900 reads KE, where KE = 0 for normal-shock entropy and KE = 2 for variable entropy. These are the only allowable values for KE.

Description of New Output Parameters

Near the beginning of the output from the program, the parameter KE, P2 (p_2), RHO2 (ρ_2), H2 (h_2), B, BB ($\bar{B}$), RPER ($R_{T,b}$), RTB ($\bar{R}_T$), DOR (Δ/R_T), and NO. OF ITER (number of iterations for calculating the shock standoff distance) are printed. In addition, the following 8 parameters are printed for each position along a streamline:

GBK — local shock angle, $\bar{\Gamma}$ $(\bar{\xi},\bar{\beta})$

GBL — shock angle where streamline at boundary layer edge crossed the shock, $\bar{\Gamma}$ $(\bar{\beta},\Psi)$

PSH — pressure aft of shock angle GBL, p_{sh} $(\bar{\beta},\Psi)(lb/ft^2)$

PSHK — pressure aft of local shock angle GBK, p_{sh} $(\bar{\xi},\bar{\beta})(lb/ft^2)$

PB — surface pressure for shock solution only, p_b (lb/ft^2)

PE — surface pressure for calculating heating rates, p_e (lb/ft^2)

PSS(SHK) — stream function at edge of shock layer, Ψ_{sh} (slug/sec)

PSS — stream function at position where streamline at boundary layer edge crossed the shock, Ψ_{BL} (slug/sec)

REFERENCES

1. DeJarnette, F. R.: Calculation of Inviscid Surface Streamlines and Heat Transfer on Shuttle Type Configurations. Part I. NASA CR-111921, August 1971.

2. DeJarnette, F. R.; and Hamilton, H. H.: Inviscid Surface Streamlines and Heat Transfer on Shuttle Type Configurations. AIAA Paper No. 72-703, presented at the AIAA 5th Fluid and Plasma Dynamics Conference, Boston, Mass., June 26-28, 1972.

3. DeJarnette, F. R.; and Jones, M. H.: Calculation of Inviscid Surface Streamlines and Heat Transfer on Shuttle Type Configurations. Part II - Description of Computer Program. NASA CR-111922, August 1971.

4. Maslen, S. H.: Inviscid Hypersonic Flow Past Smooth Symmetric Bodies. AIAA Journal, June 1964, pp. 1055-1061.

5. Maslen, S. H.: Asymmetric Hypersonic Flow. RIAS Technical Report 71-27C (NASA CR-2123), September 1971.

6. Hayes, W. D.; and Probstein, R. F.: Hypersonic Flow Theory, Vol. I. Academic Press, 1965.

7. Cohen, N. B.: Correlation Formulas and Tables of Density and Some Transport Properties of Equilibrium Dissociating Air for Use in Solutions of the Boundary Layer Equations. NASA TN D-194, 1960.

8. Beckwith, I. E.; and Cohen, N. B.: Application of Similar Solutions to Calculation of Laminar Heat Transfer on Bodies with Yaw and Large Pressure Gradient in High-Speed Flow. NASA TN D-625, 1961.

9. Reshotko, E.; and Tucker, M.: Approximate Calculation of the Compressible Turbulent Boundary Layer with Heat Transfer and Arbitrary Pressure Gradient. NACA TN 4154, 1957.

10. Cleary, J. W.: Effects of Angle of Attack and Bluntness on Laminar Heating-Rate Distributions of a 15° Cone at a Mach Number of 10.6. NASA TN D-5450, 1969.

11. Hillsamer, M. E.; and Rhudy, J. P.: Heat-Transfer and Shadowgraph Tests of Several Elliptical Lifting Bodies at Mach 10. AEDC-TDR-64-19, U. S. Air Force, 1964.

12. Rakich, J. V.; and Kutler, Paul: Comparison of Characteristics and Shock Capturing Methods with Application to the Space Shuttle Vehicle. AIAA Paper No. 72-191. Presented at the AIAA 10th Aerospace Sciences Meeting, San Diego, California, Jan. 17-19, 1972.

TABLE 1. STAGNATION LINE STANDOFF DISTANCE COMPARED WITH MASLEN'S RESULTS

ρ_2/ρ_∞	$\bar{B}$	$\Delta/\bar{R}_T$ By Maslen's Method (Ref. 5)	$\Delta/\bar{R}_T$ (Present Method)
6	2	.06669 ± .001169	.06530
20	2	.02462 ± .000328	.02462
50	2	.01098 ± .0001195	.01090
200	2	.003046 ± .00002968	.003022
6	1	.1 ± 0.0	.1010
6	2	.06669 ± .001169	.06530
6	3	.05008 ± .001610	.04795
6	5	.03349 ± .001963	.03104

NOTE: 1) For all Calculations $\gamma = 1.4$, but the normal shock density ratio is assumed to be separately varied as shown.

2) The $\bar{B}$ used herein is greater than Maslen's B; $\bar{B} = B_{Maslen} + 1$.

TABLE 2. DATA FOR BLUNTED 2:1 ELLIPTICAL CONE CASES

	p_s (lb/in^2)	T_s (°R)	M_∞	p_∞ (lb/ft^2)	T_∞ (°R)
1)	200	1660	10.04	0.6395	81.20
2)	750	1800	10.13	2.2766	87.31
3)	2000	1900	10.19	5.9184	92.00

	V_∞ (ft/sec)	Re_∞/ft	$Re_{\infty,N}$	γ	ζ_w
1)	4434.40	$.313 \times 10^6$	2.61×10^4	1.4	.27354
2)	4639.42	1.007×10^6	8.39×10^4	1.4	.25010
3)	4790.61	2.42×10^6	2.02×10^5	1.4	.23470

TABLE 3. BODY SHAPE FOR SPACE SHUTTLE ORBITER WITHOUT CANOPY, LENGTH L = 1.0 FT.

Coefficients a_i for

		y, Windward			
Segment	x_1	a_o	a_1	a_2	a_3
1	.05	.025	.26795	-4.0678	30.1760
2	.10	.032	.08749	- .4499	.68725
3	.30	.037	-.010	0	0
4	.50	.035	-.010	0	0
5	.70	.033	-.010	0	0
		y, Leeward			
Segment	x_1	a_o	a_1	a_2	a_3
1	.05	.025	.26795	0	0
2	.10	.0384	.26795	.12770	-.88725
3	.30	.090	.21256	-.22505	-.4385
4	.50	.120	.06993	-.0366	-.31525
5	.70	.130	.01746	.02121	-.07952
		z, Side			
Segment	x_1	a_o	a_1	a_2	a_3
1	.05	.025	.26795	-1.0446	1.7120
2	.10	.036	.17633	- .3383	.90825
3	.30	.065	.150	0	0
4	.50	.095	.150	- .02935	.77175
5	.70	.130	.23078	1.3697	-1.7605

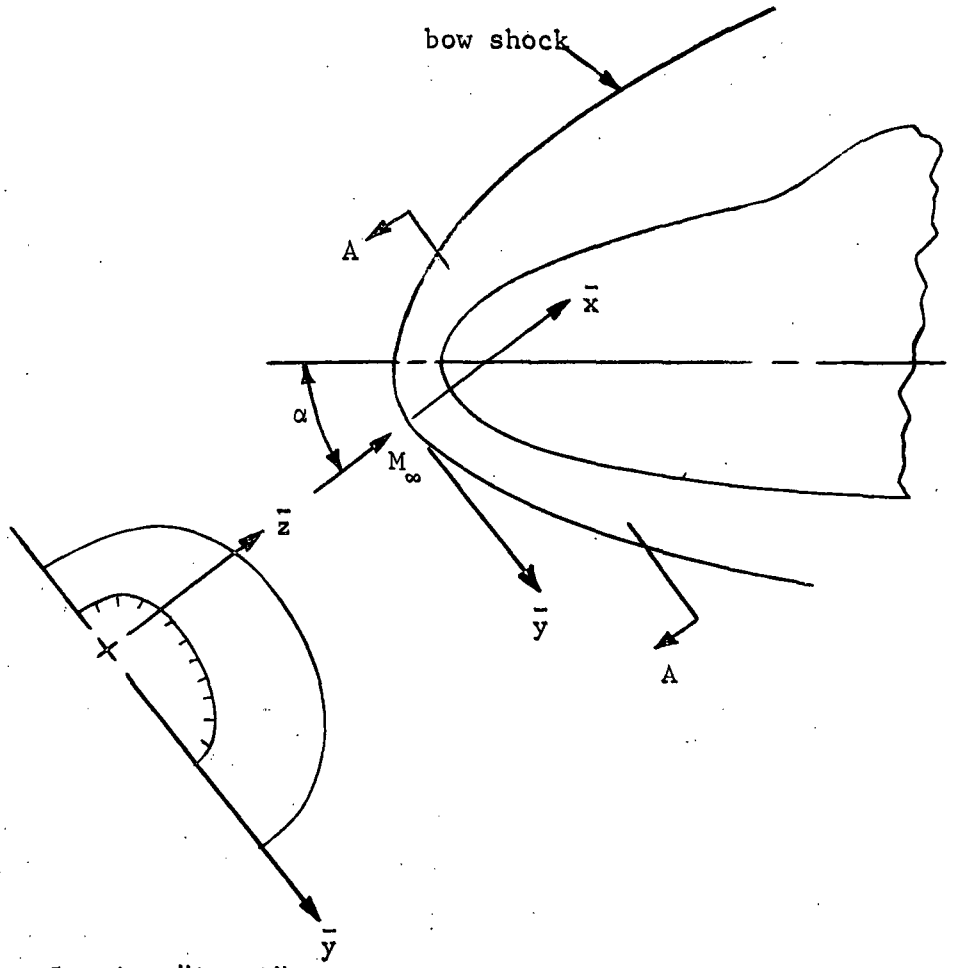

Figure 1. Shock-oriented coordinate system.

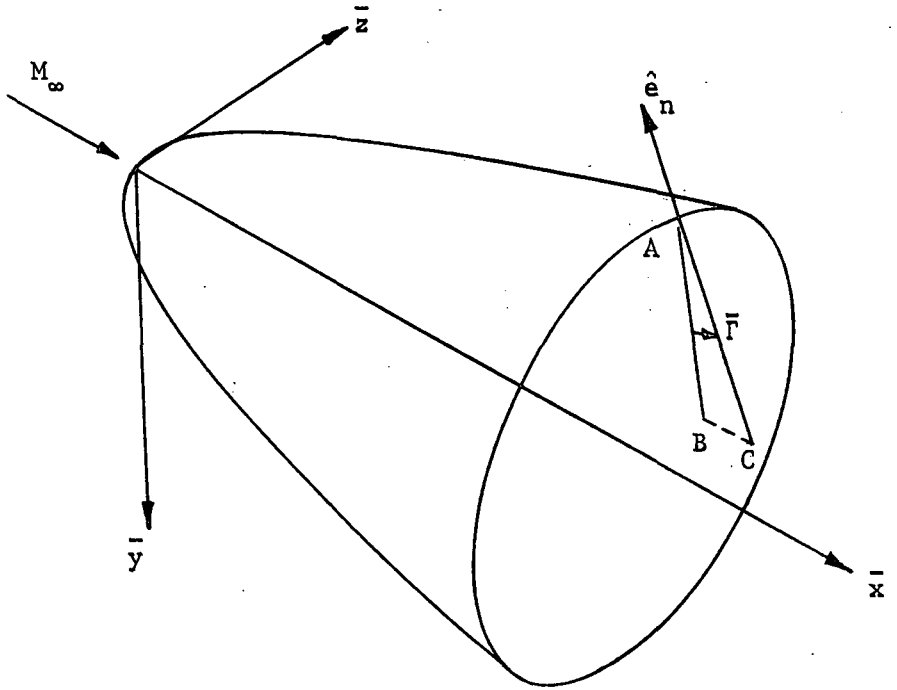

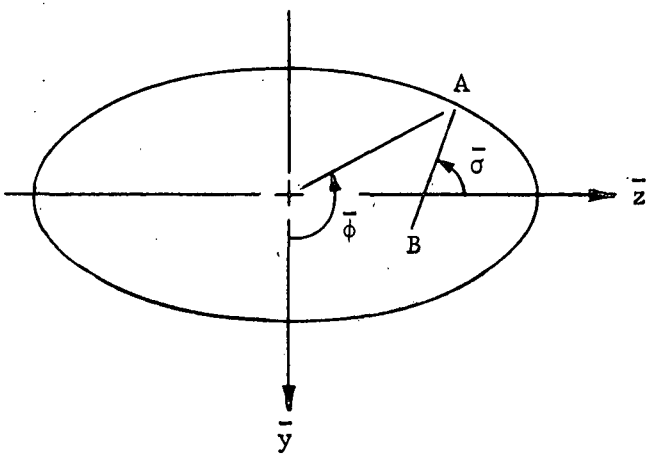

Cross section of shock
(viewed from rear)

$\overline{AC}$ is normal to shock wave at A

$\overline{AB}$ is projection of $\overline{AC}$ onto cross-sectional plane

Figure 2. Geometry of shock-wave angles $\bar{\Gamma}$ and $\bar{\sigma}$.

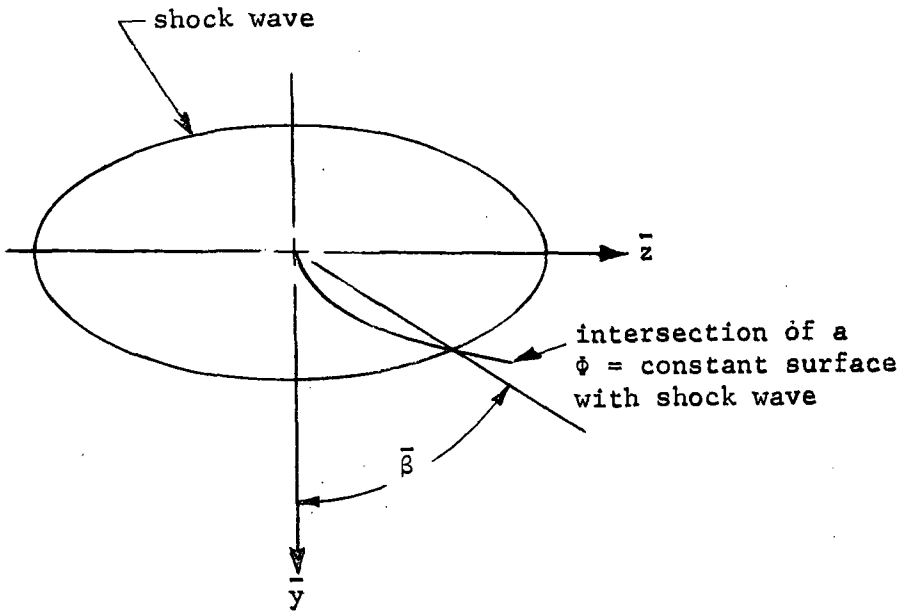

Cross section of shock surface
at $\bar{x} = \bar{\varepsilon}^2/(2\bar{R}_T)$

Figure 3. Method for assigning values to coordinate $\bar{\beta}$ near stagnation line.

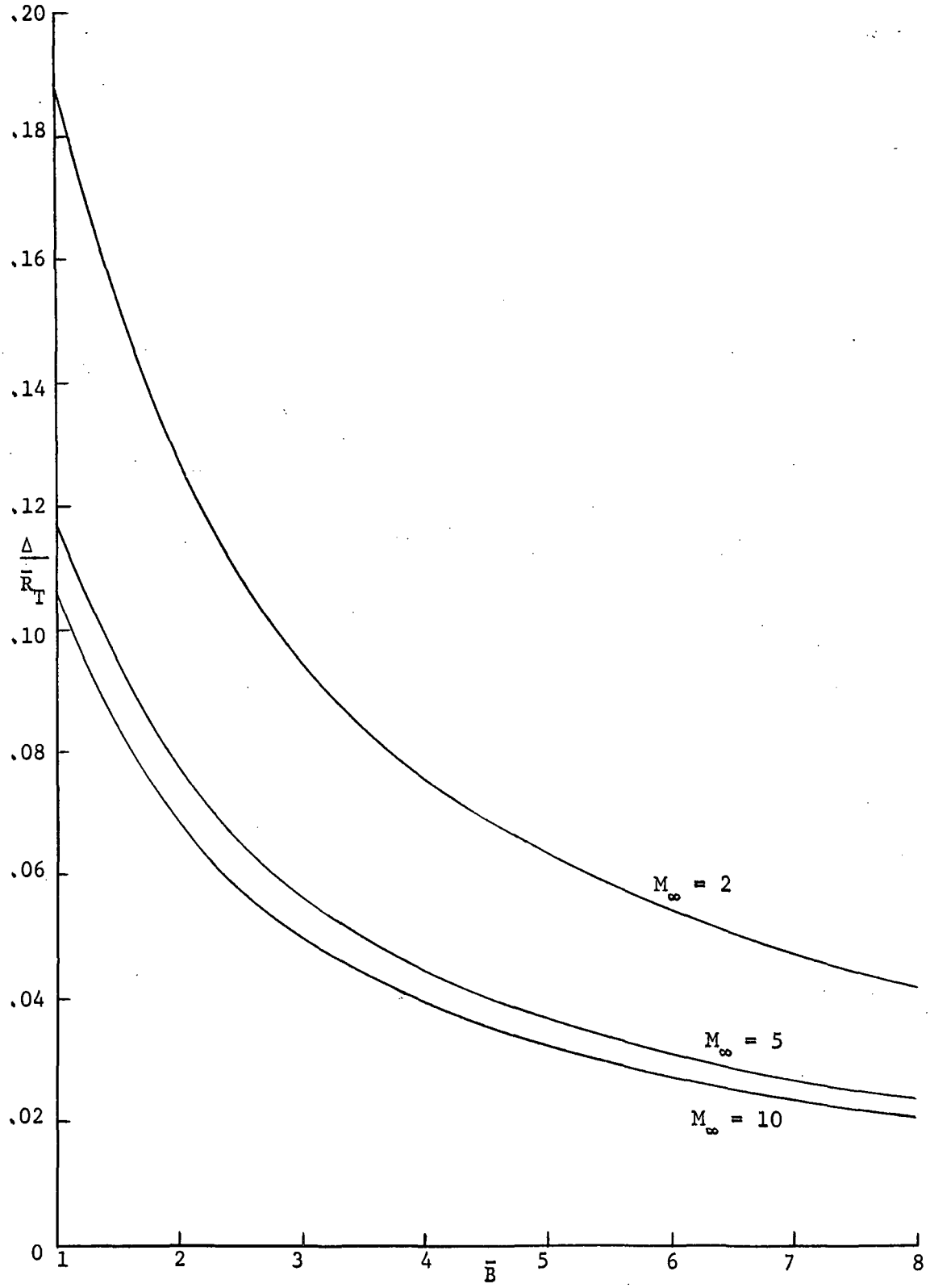

Figure 4. Three-dimensional shock standoff distance, $\gamma = 1.4$.

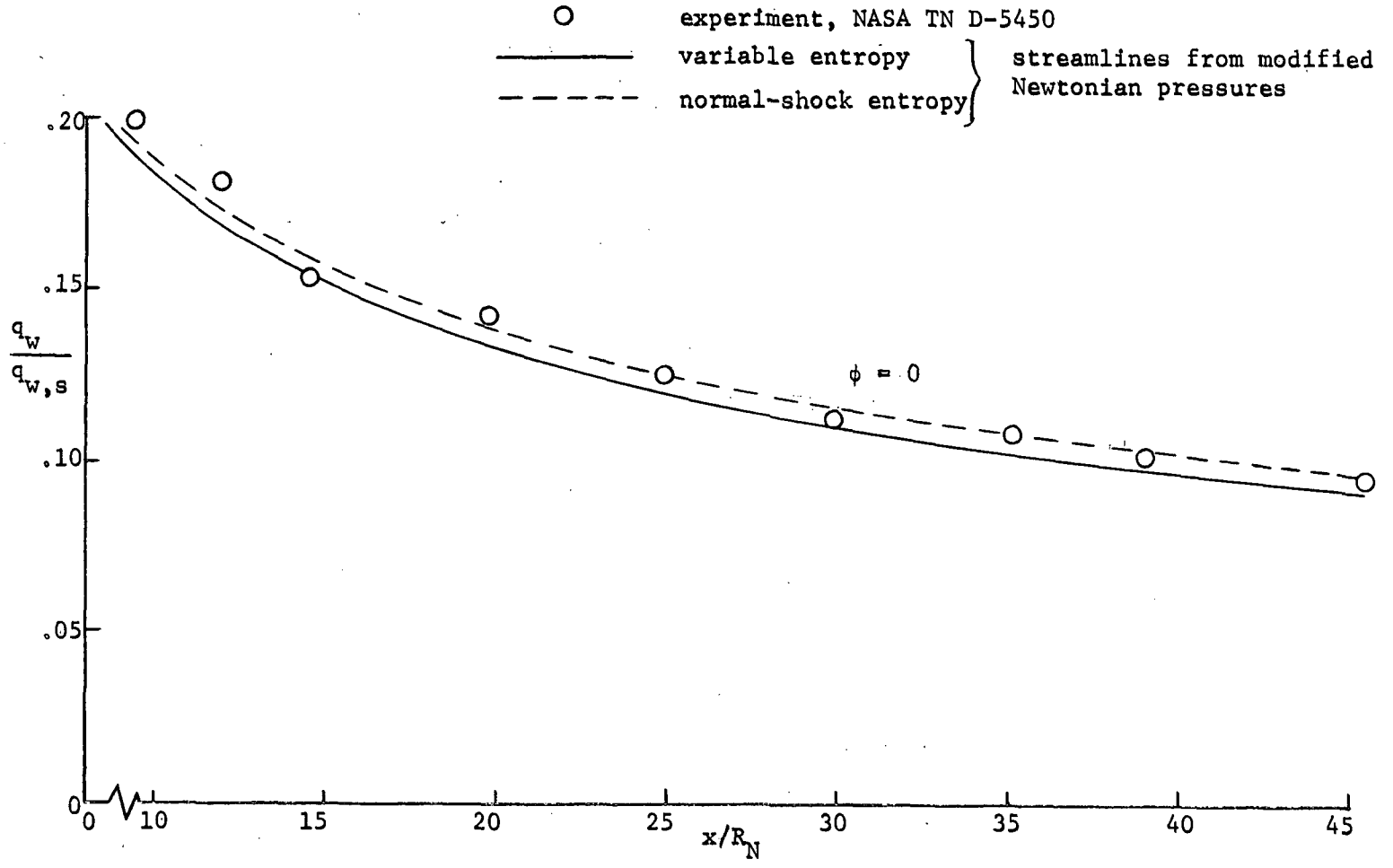

Figure 5. Heat-transfer distribution on blunt 15° half-angle cone, $\alpha = 20°$, $M_\infty = 10.6$, and $Re_{\infty,N} = 3.75 \times 10^4$.

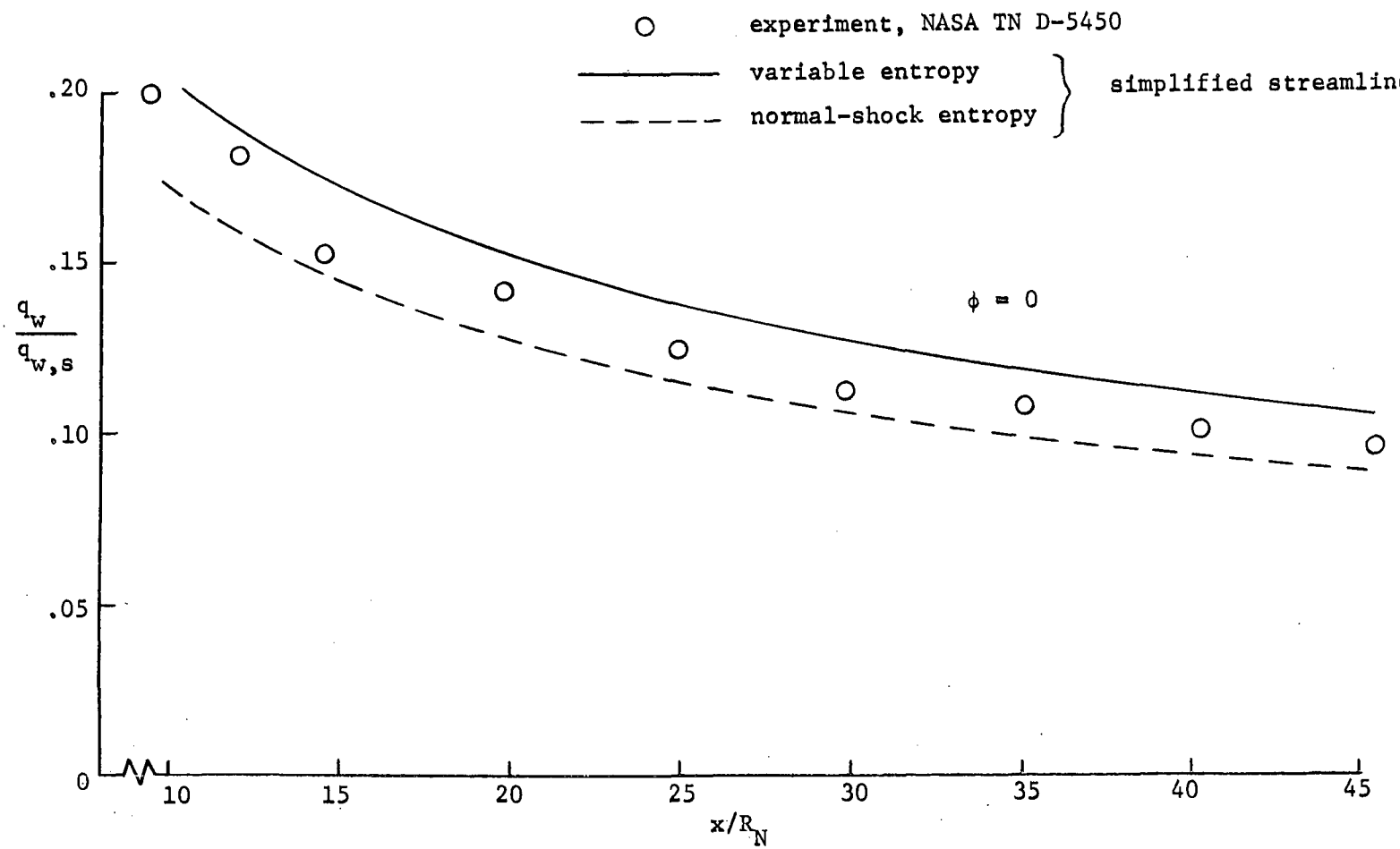

Figure 6. Heat-transfer distribution on blunt 15° half-angle cone, $\alpha = 20°$, $M_\infty = 10.6$, and $Re_{\infty,N} = 3.75 \times 10^4$.

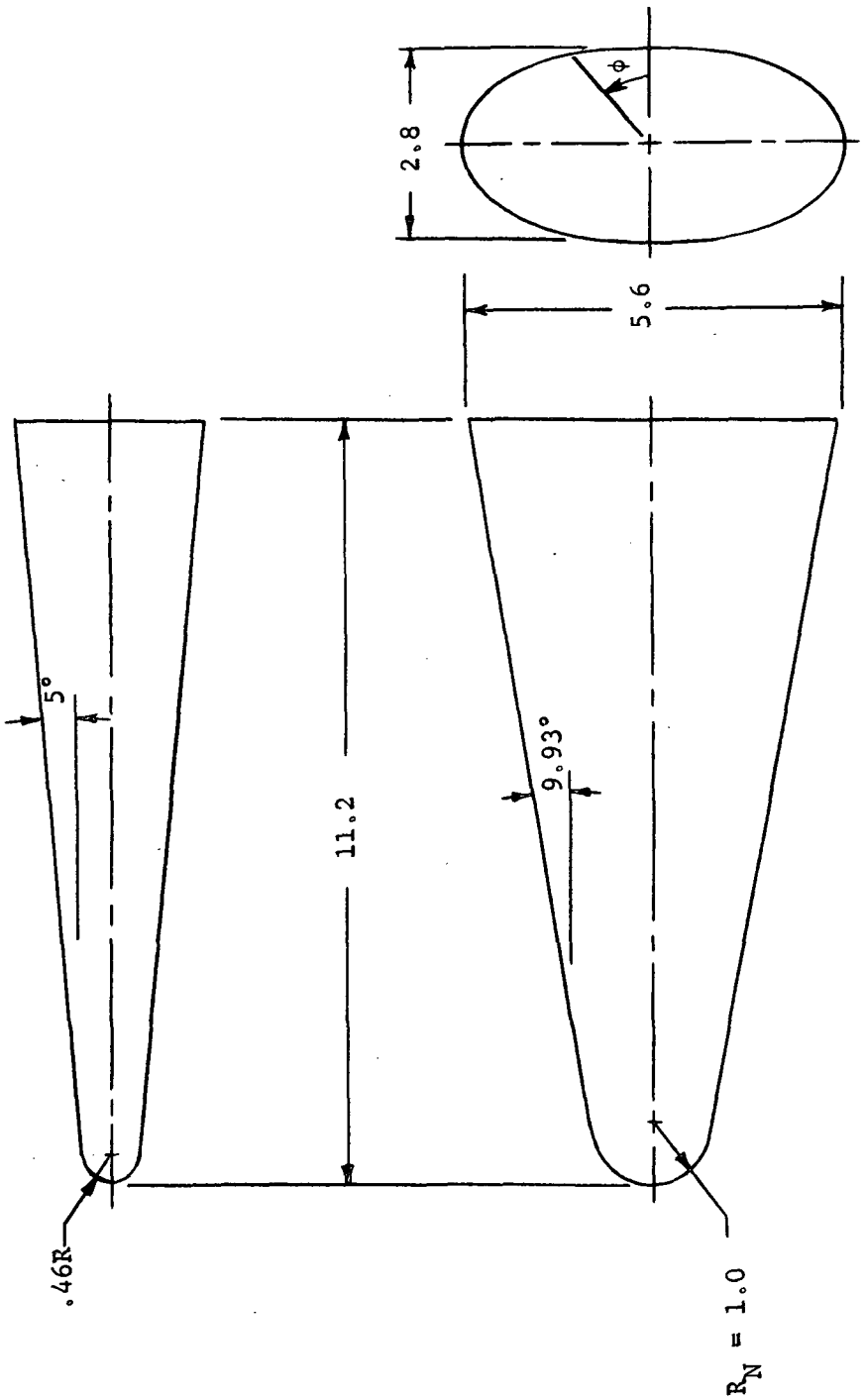

Figure 7. Details of blunted 2:1 elliptical cone model.

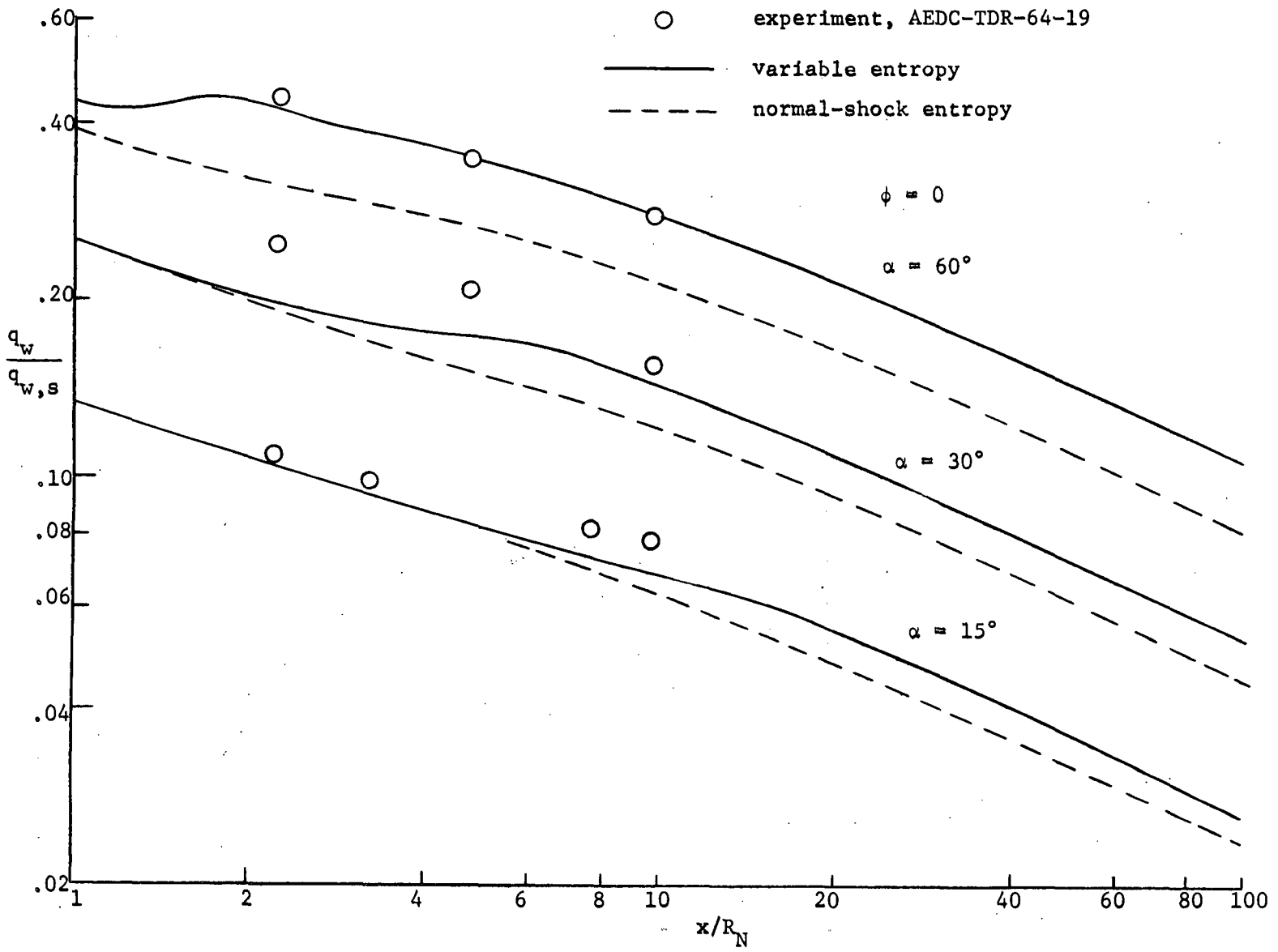

Figure 8. Heat-transfer distribution on a blunted 2:1 elliptical cone, $M_\infty = 10$, $Re_{\infty,N} = 8.39 \times 10^4$.

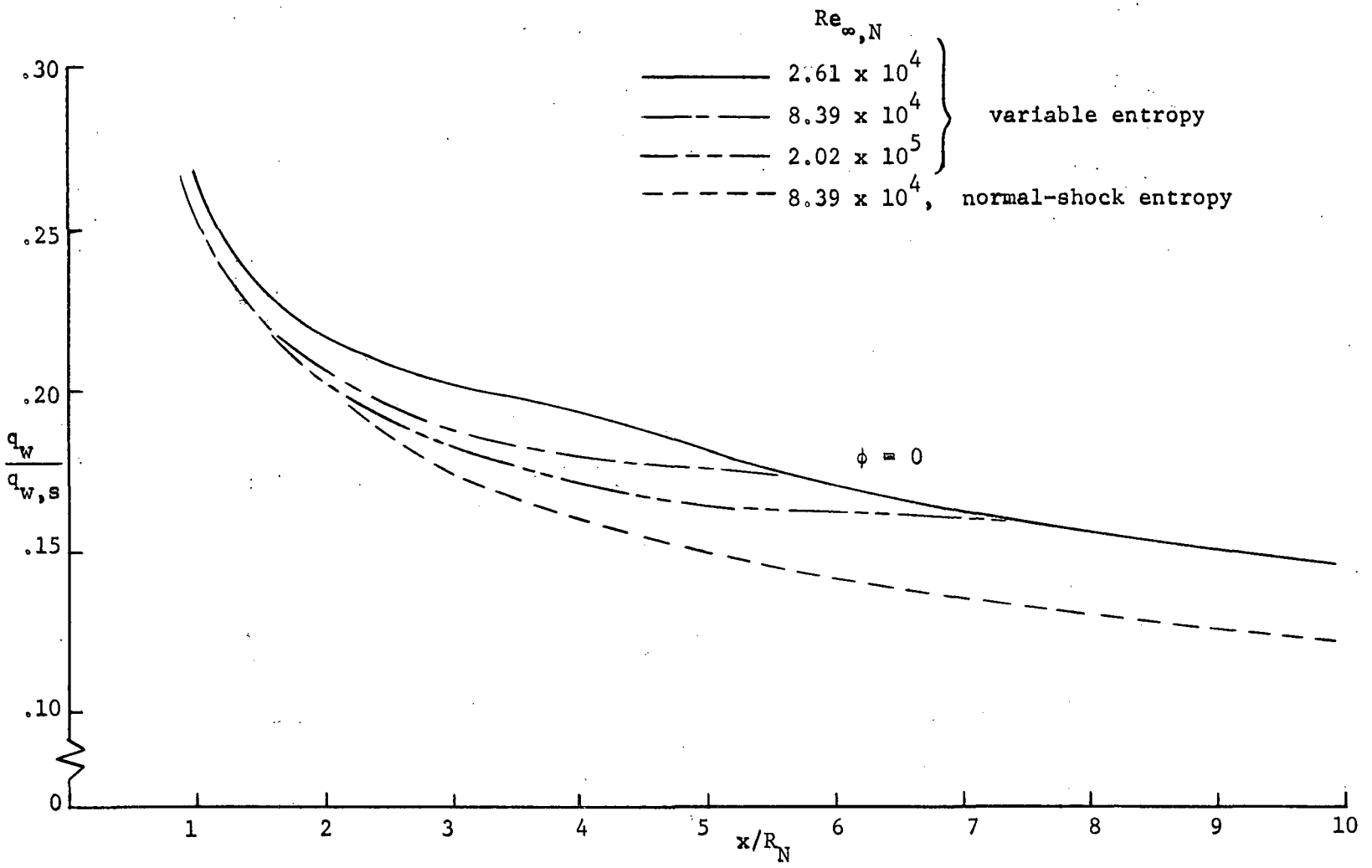

Figure 9. Effect of Reynolds number on the heat-transfer distribution on a blunted 2:1 elliptical cone, $\alpha = 30°$, $M_\infty = 10$.

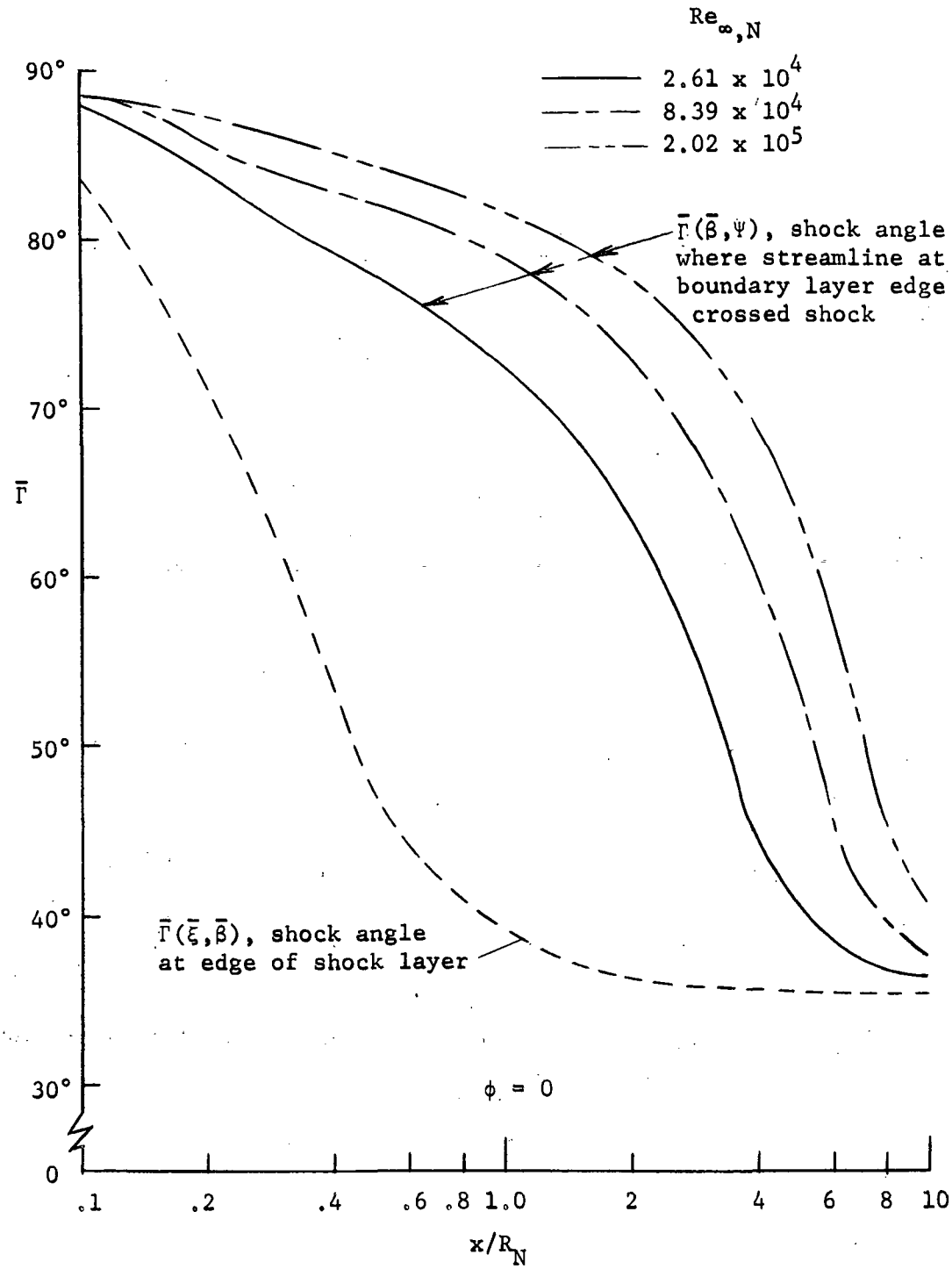

Figure 10. Shock-wave angle distribution on blunted 2:1 elliptical cone, $\alpha = 30°$, $M_\infty = 10$.

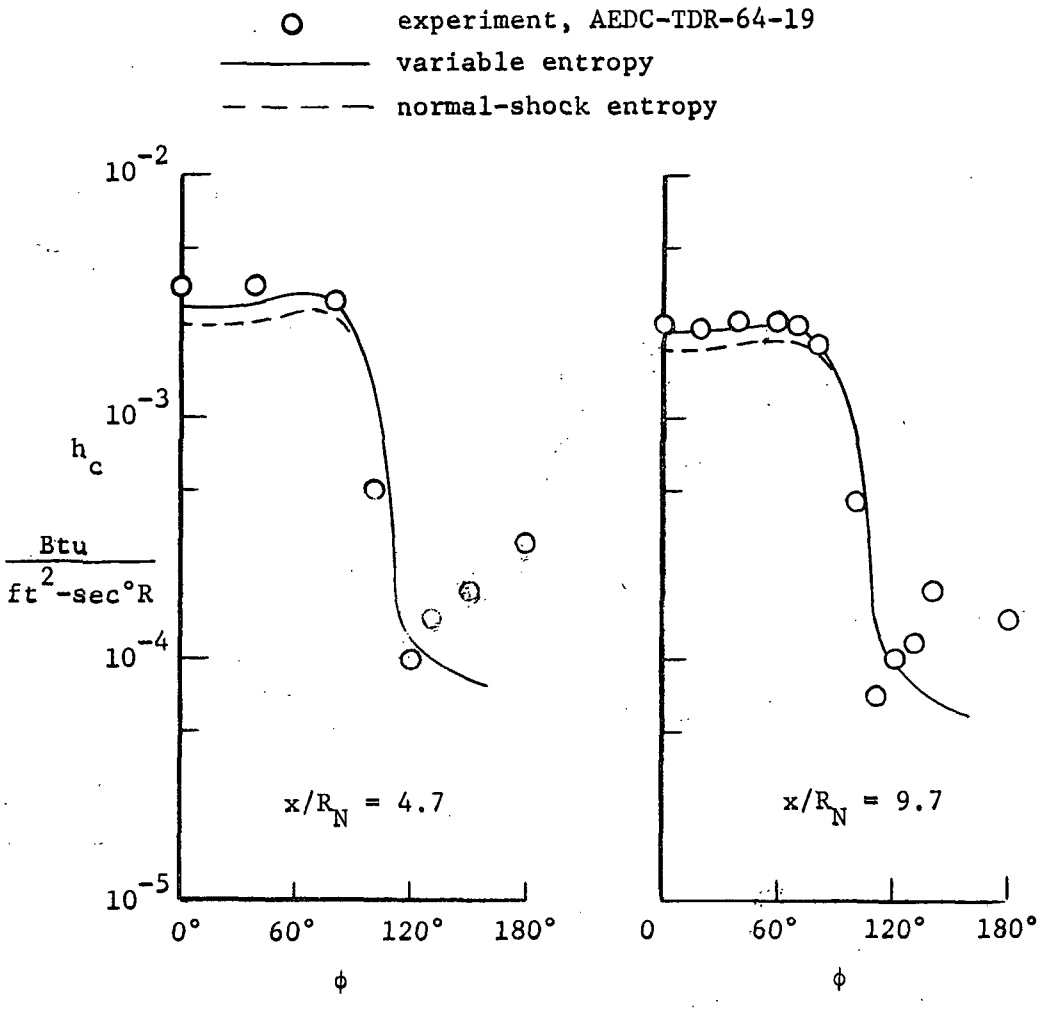

Figure 11. Circumferential heat-transfer distribution on a blunted 2:1 elliptical cone, $\alpha = 30°$, $M_\infty = 10$, $Re_{\infty,N} = 8.39 \times 10^4$.

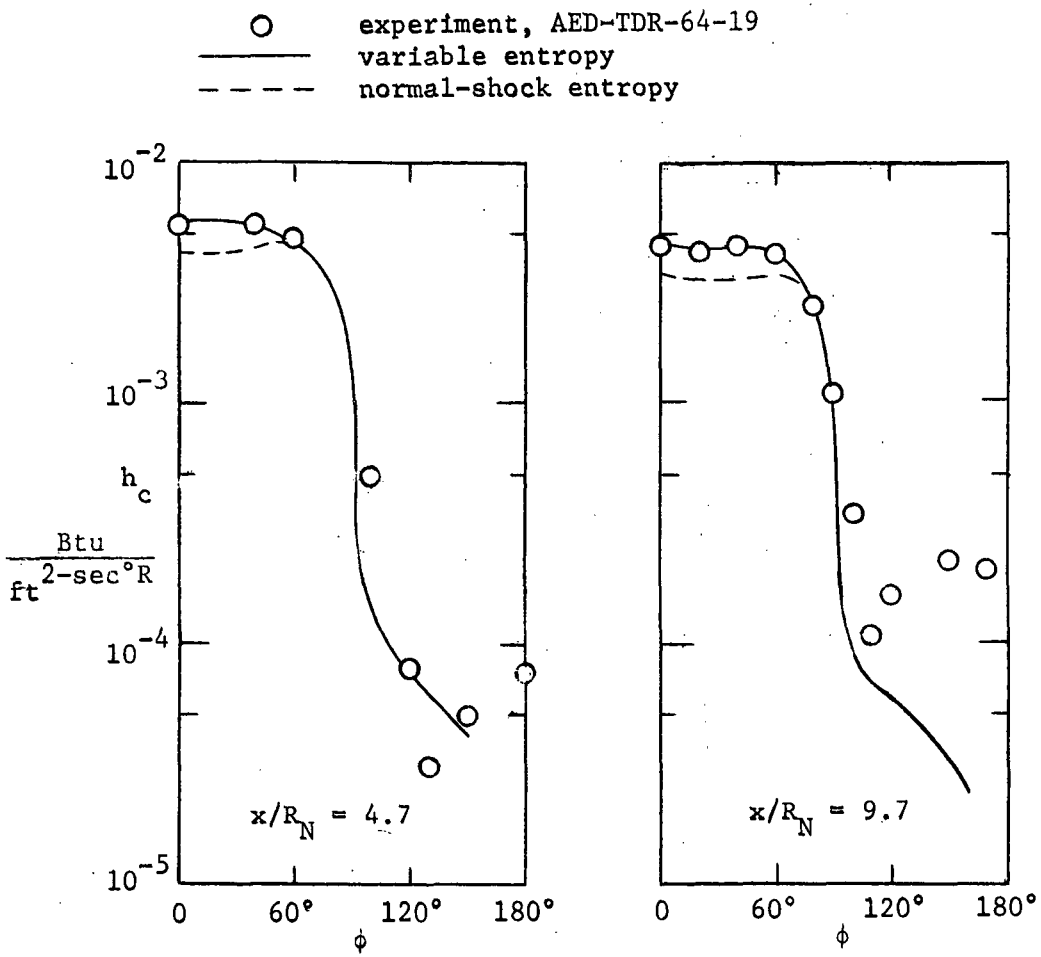

Figure 12. Circumferential heat-transfer distribution on blunted 2:1 elliptical cone, $\alpha = 60°$, $M_\infty = 10$, $Re_{\infty,N} = 8.39 \times 10^4$.

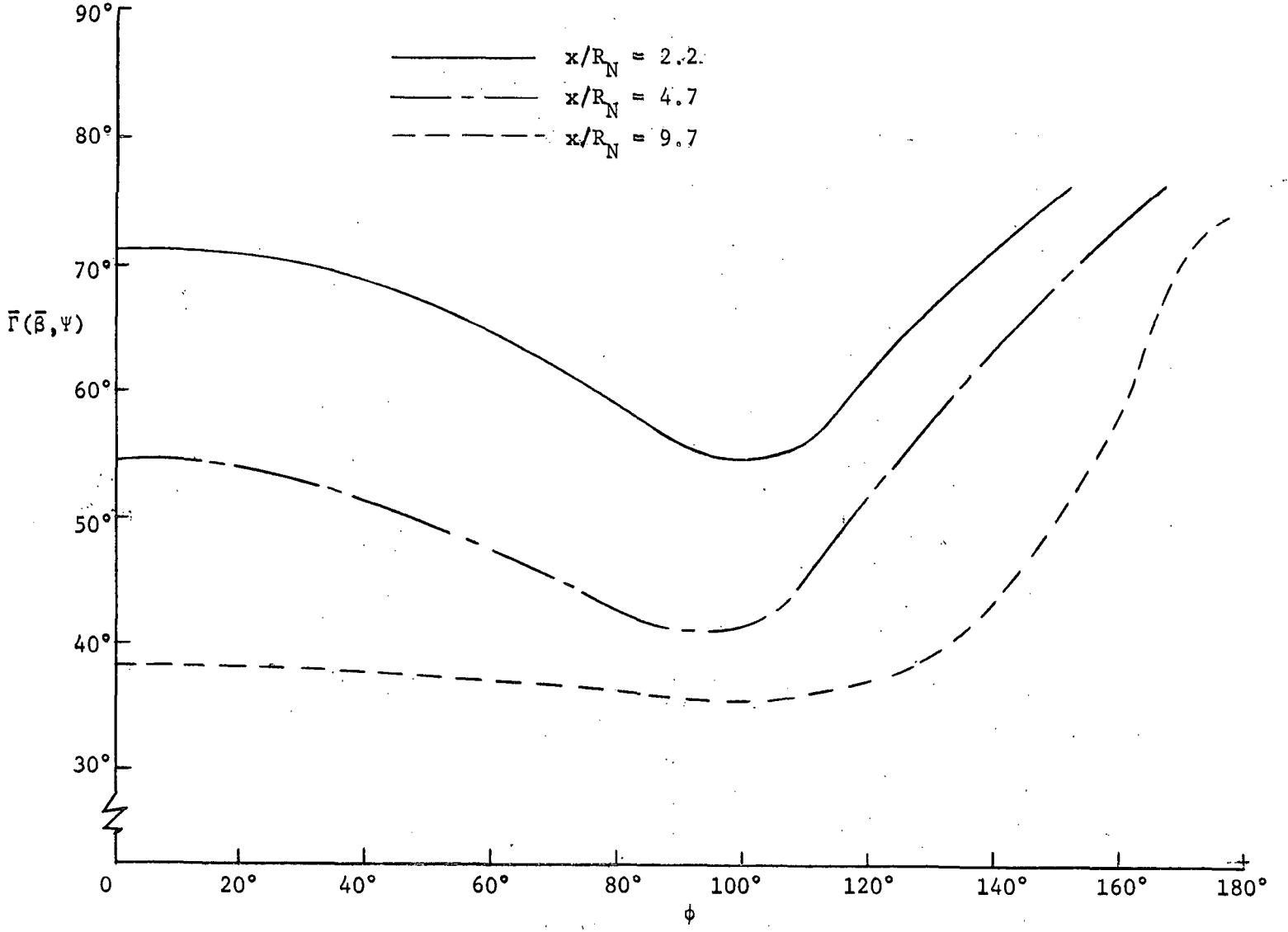

Figure 13. Circumferential variation of shock angle on blunted 2:1 elliptical cone, $\alpha = 30°$, $M_\infty = 10$, $Re_{\infty,N} = 8.39 \times 10^4$.

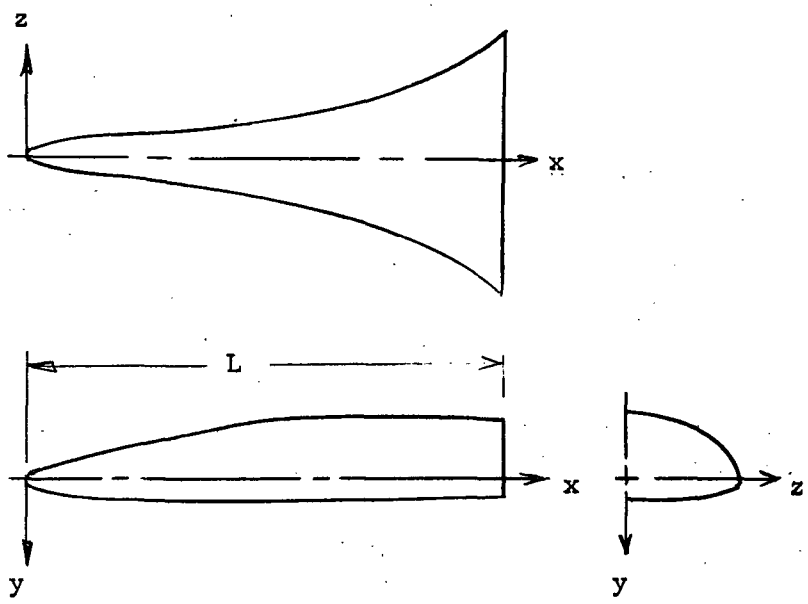

Figure 14. Typical space shuttle orbiter without canopy.

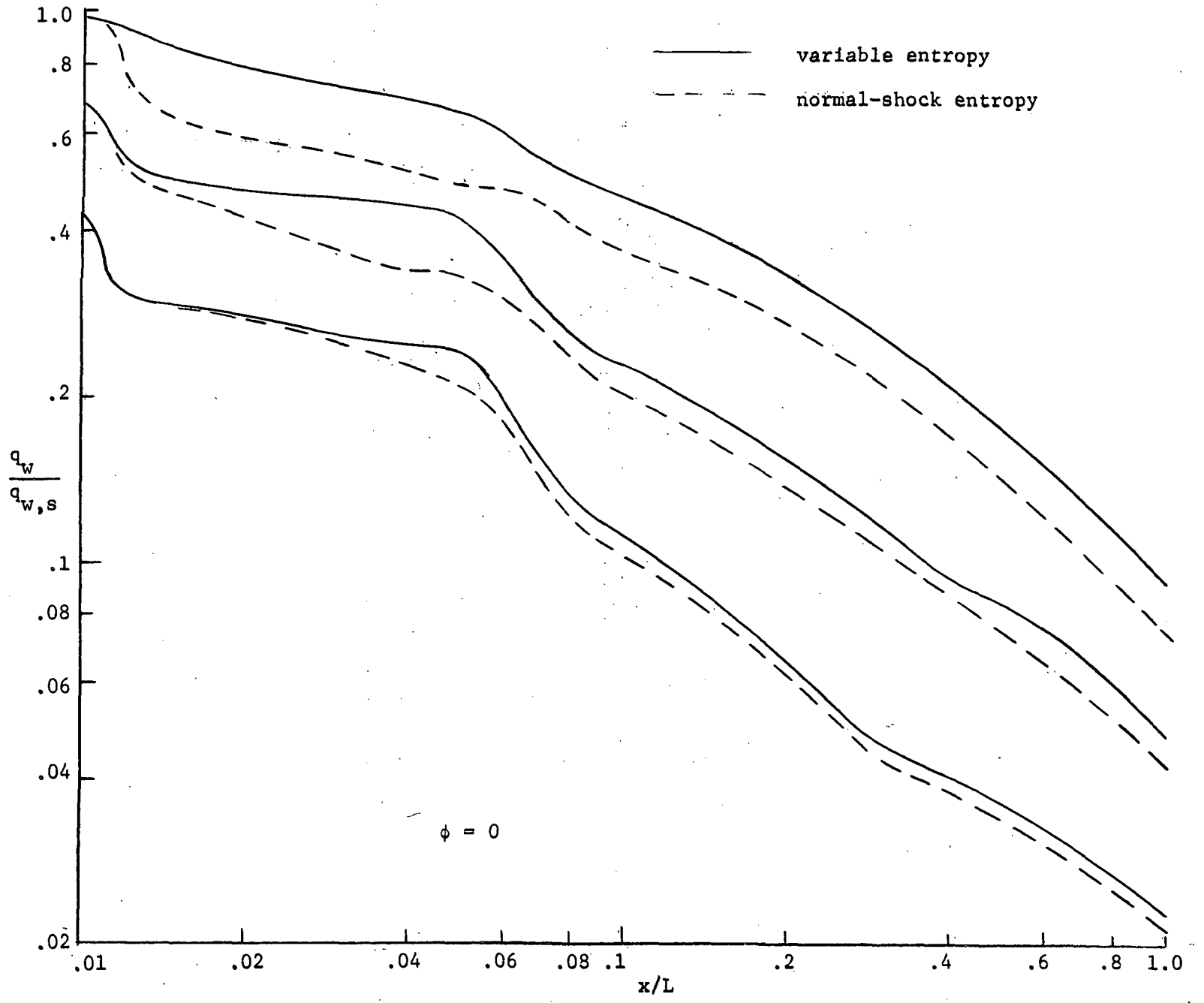

Figure 15. Heat-transfer distribution on typical space shuttle orbiter, $M_\infty = 10$, $Re_{\infty,N} = 1.5 \times 10^4$.

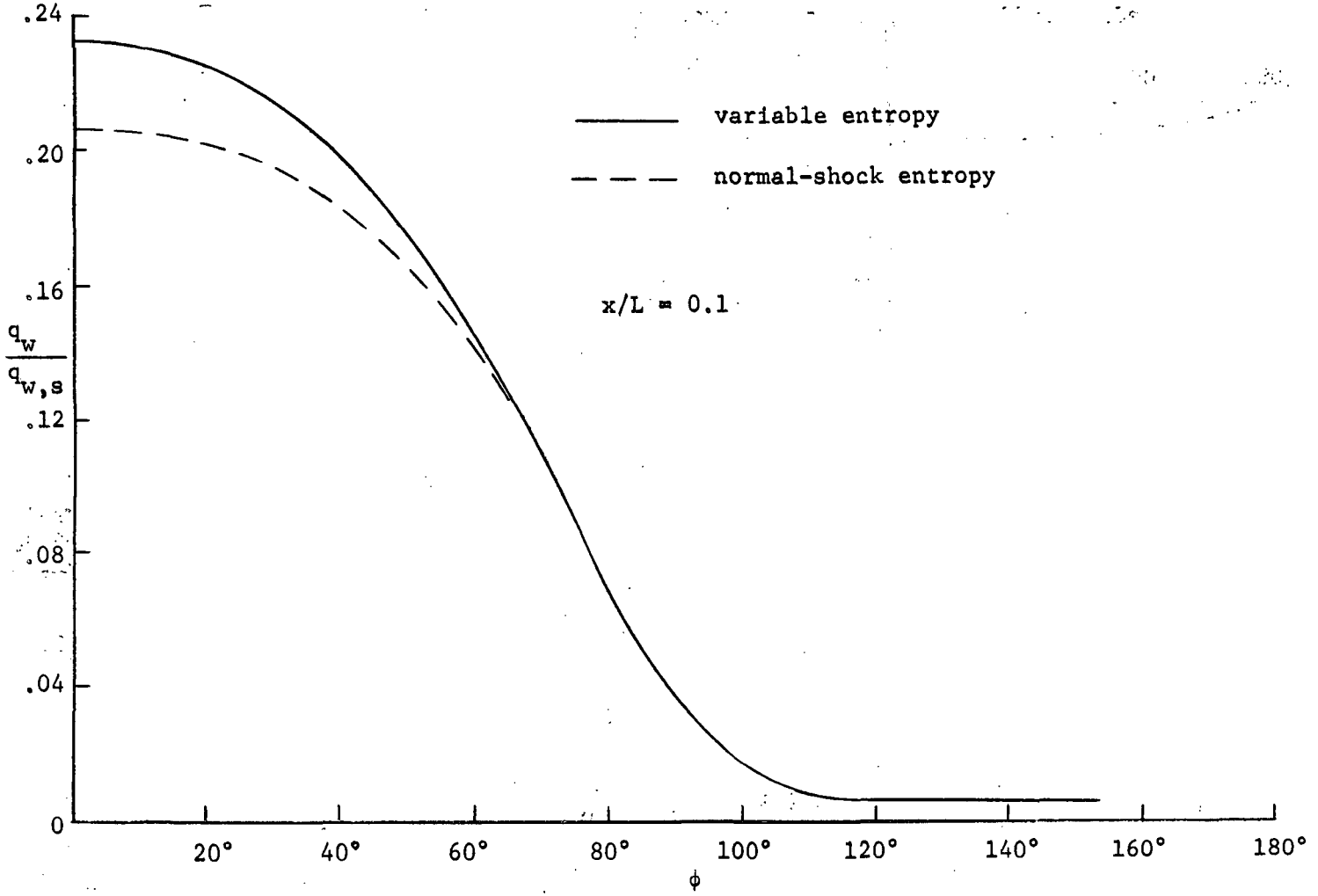

Figure 16. Circumferential heat-transfer distribution on typical space shuttle orbiter, $M_\infty = 10$, $\alpha = 30°$, $Re_{\infty,N} = 1.5 \times 10^4$.

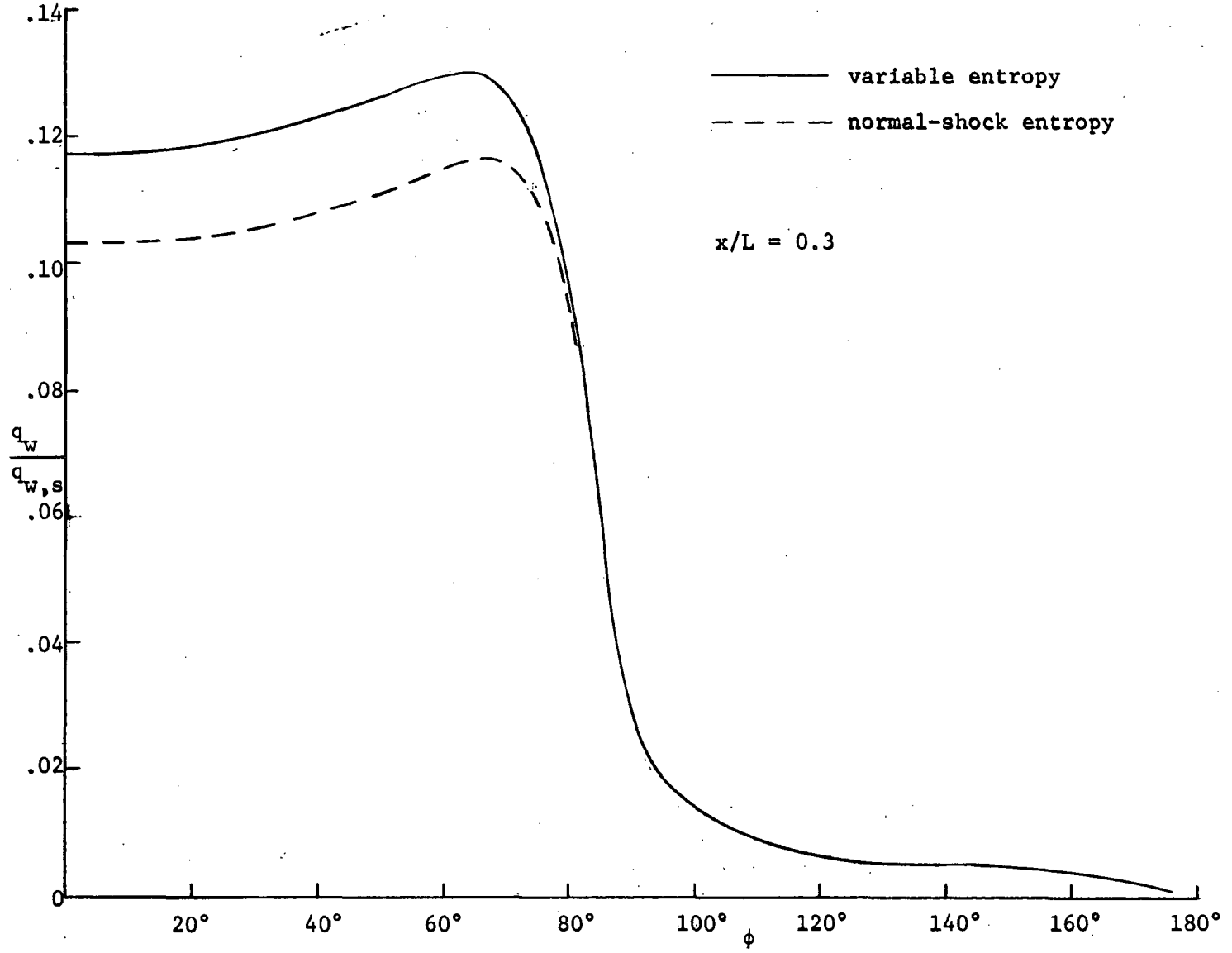

Figure 17. Circumferential heat-transfer distribution on typical space shuttle orbiter, $M_\infty = 10$, $\alpha = 30°$, $Re_{\infty,N} = 1.5 \times 10^4$.

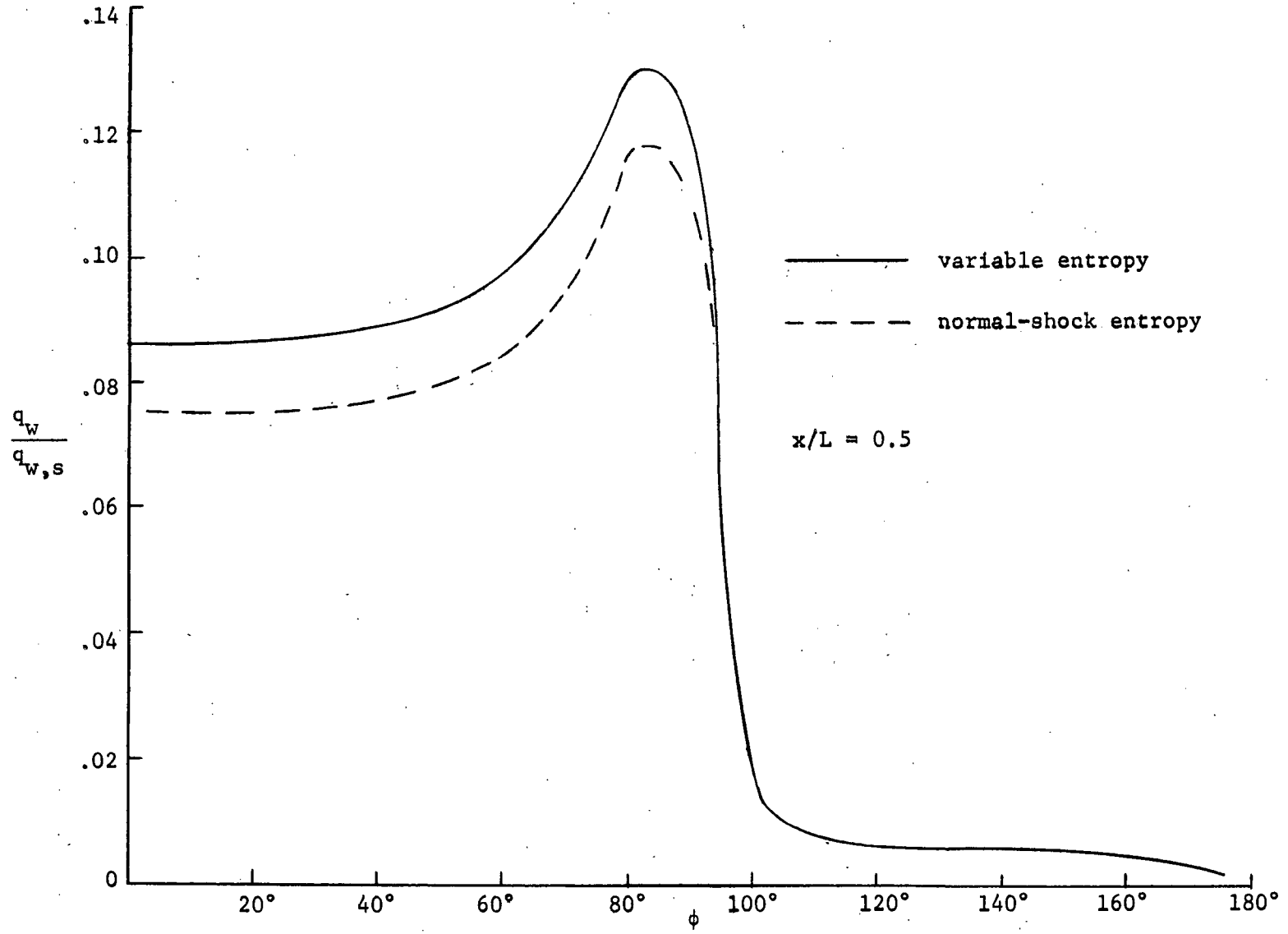

Figure 18. Circumferential heat-transfer distribution on typical space shuttle orbiter, $M_\infty = 10$, $\alpha = 30°$, $Re_{\infty,N} = 1.5 \times 10^4$.

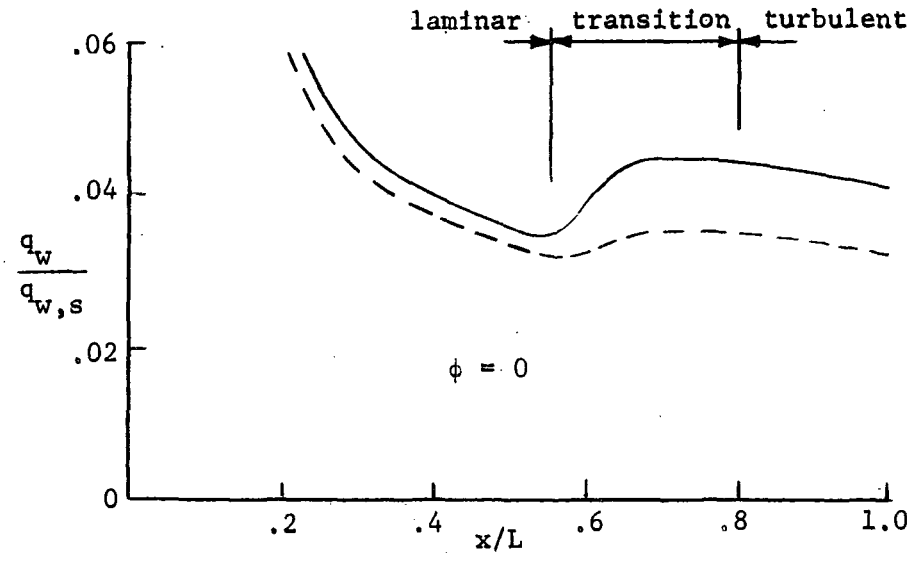

(a) $\alpha = 15°$

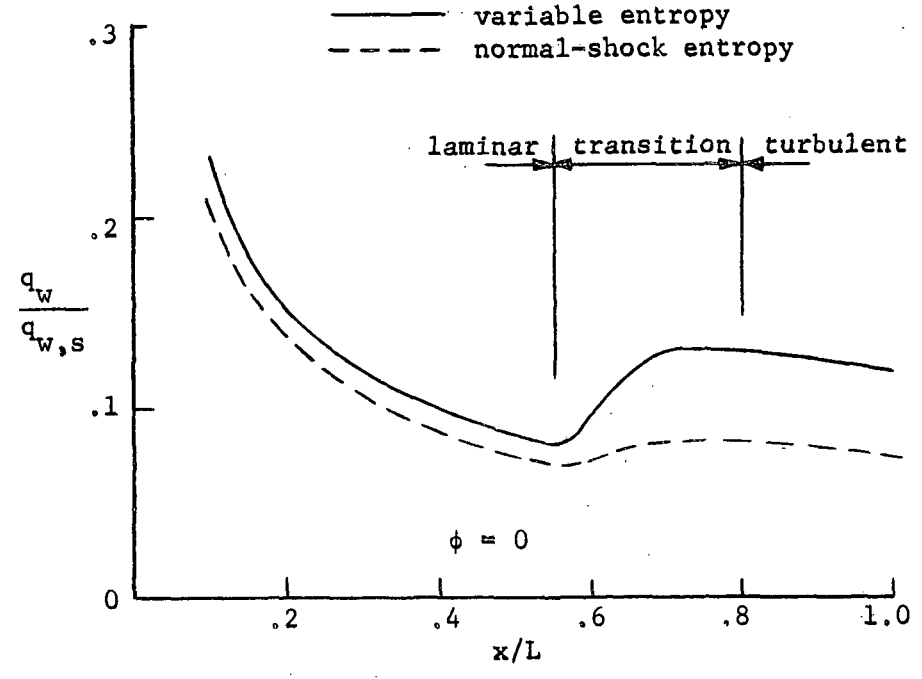

(b) $\alpha = 30°$

Figure 19. Laminar, transitional, and turbulent heat-transfer distribution on typical space shuttle orbiter, $M_\infty = 10$, $Re_{\infty,N} = 1.5 \times 10^4$.